Stoichiometric ratios for biotics and xenobiotics capture effective metabolic coupling to re(de)fine biodegradation

Nolte, T.M.; Peijnenburg, W.J.G.M.; Rios- Miguel, A.B.; Zhang, Y; Hendriks, A.J.

Water Research 217 (2022) 118333

Contents lists available at ScienceDirect

Water Research

journal homepage: www.elsevier.com/locate/watres

Stoichiometric ratios for biotics and xenobiotics capture effective metabolic coupling to re(de)fine biodegradation

Tom M. Nolte [a,*], Willie J.G.M. Peijnenburg [b,e], Ana B. Rios- Miguel [c], Ya-nan Zhang [d], A. Jan Hendriks [a]

[a] Radboud University Nijmegen, Department of Environmental Science, Institute for Water and Wetland Research, 6500 GL Nijmegen, the Netherlands
[b] Institute of Environmental Sciences (CML), Leiden University, PO Box 9518, 2300 RA, Leiden, the Netherlands
[c] Radboud University Nijmegen, Department of Microbiology, Institute for Water and Wetland Research, 6500 GL Nijmegen, the Netherlands
[d] School of Environment, Northeast Normal University, NO. 2555 Jingyue Street, Changchun, Jilin 130117, China
[e] National Institute of Public Health and the Environment, PO Box 1, 3720 BA Bilthoven, the Netherlands

ARTICLE INFO

Keywords:
Biodegradation
Wastewater
Surface water
Organic pollutants
Stoichiometry
Metabolism

ABSTRACT

Preserving human and environmental health requires anthropogenic pollutants to be biologically degradable. Depending on concentration, both nutrients and pollutants induce and activate metabolic capacity in the endemic bacterial consortium, which in turn aids their degradation. Knowledge on such 'acclimation' is rarely implemented in risk assessment cost-effectively. As a result, an accurate description of the mechanisms and kinetics of biodegradation remains problematic.

In this study, we defined a yield 'effectivity', comprising the effectiveness at which a pollutant (substrate) enhances its own degradation by inducing (biomass) cofactors involved therein. Our architecture for calculation represents the interplay between concentration and metabolism via both stoichiometric and thermodynamic concepts. The calculus for yield 'effectivity' is biochemically intuitive, implicitly embeds co-metabolism and distinguishes 'endogenic' from 'exogenic' substances' reflecting various phenomena in biodegradation and biotransformation studies.

We combined data on half-lives of pollutants/nutrients in wastewater and surface water with transition-state rate theory to obtain also experimental values for effective yields. These quantify the state of acclimation: the portion of biodegradation kinetics attributable to (contributed by) 'natural metabolism', in view of similarity to natural substances. Calculated and experimental values showed statistically significant correspondence. Particularly, carbohydrate metabolism and nucleic acid metabolism appeared relevant for acclimation ($R^2 = 0.11–0.42$), affecting rates up to $10^{4.9(\pm 0.7)}$ times: under steady-state acclimation, a compound stoichiometrically identical to carbohydrates or nucleic acids, is $10^{3.2}$ to $10^{4.9}$ times faster aerobically degraded than a compound marginally similar.

Our new method, simulating (contribution by) the state of acclimation, supplements existing structure-biodegradation and kinetic models for predicting biodegradation in wastewater and surface water. The accuracy of prediction may increase when characterizing nutrients/co-metabolites in terms of, e.g., elemental analysis. We discuss strengths and limitations of our approach by comparison to empirical and mechanism-based methods.

1. Introduction

After use, anthropogenic (e.g., agricultural, industrial, household) chemicals often enter our environment. This driving force of pollution affects human health as well as biodiversity in soil and water ecosystems worldwide (Posthuma et al., 2019b; Vrijheid et al., 2016; Wang et al., 2021). Evaluating hazards involves understanding the fate of chemicals and their mixtures (De Zwart and Posthuma, 2005; Sathishkumar et al., 2020, 2021), relevant for developing less persistent "green" or "benign-by-design" chemicals (Nolte et al., 2020a; Rucker and Kummerer, 2012).

Among many remediation strategies (Kumar et al., 2020; Ma et al.,

* Corresponding author.
E-mail address: t.nolte@science.ru.nl (T.M. Nolte).

https://doi.org/10.1016/j.watres.2022.118333
Received 15 January 2022; Received in revised form 7 March 2022; Accepted 19 March 2022
Available online 26 March 2022

2021; Mendes-Felipe et al., 2022; Sharma et al., 2021), biological degradation removes anthropogenic pollutants from the environment in a cost- and energy-efficient way, so as to reduce human exposure and improve environmental quality. Moreover, proper description of biotransformation processes is essential for accurate environmental fate assessments (Directive 2000; Knott et al., 2020). Static fate models such as SimpleTreat (Struijs et al., 2020) apply half-lives or removal efficiencies, as obtained from OECD testing (Organization for Economic Co-operation and Development) (Pagga, 1997) or structure-biodegradation relationships (SBRs) (Boethling et al., 1994), to quantify the contribution of biodegradation to the overall removal and predict contaminant concentrations. Particularly, SBRs can identify and 'screen' functional groups among potentially 10.000^{+} chemicals (Leder et al., 2015) prone to biodegradation. In addition to categorial (0 or 1) SBRs (Lunghini et al., 2020), 'continuous' SBRs predict biodegradation kinetics of chemicals (in e.g., surface water, wastewater) with accuracies up to 50% (Nolte et al., 2020a, 2020c; USEPA, 2012). Attributing the remaining variance in biodegradation to a reproducible metric enables more correct assessments.

Biodegradation is often not rigorously defined (Kowalczyk et al., 2015; Rucker and Kummerer, 2012; Thouand et al., 2011): when inocula from e.g., surface waters and wastewaters are insufficiently 'standardized', testing will entail a variable biodegradation pathway as binding to receptors/enzymes, catalysis, etc. will differ. Moreover, a certain (threshold (Kovar et al., 2002)) concentration can, over time, induce acclimation, via transcription/expression of transporter/catabolic genes or even mutations and horizontal gene transfer. This would enhance specific biodegradation pathways (Fig. 1), i.e., biodegradation rate constants are thereby affected by concentration (Nolte, 2020a; Nolte and Chen, 2020a; Nolte et al., 2020b; van Bergen et al., 2020): the bacterial consortium not only degrades the pollutant/substrate S, but S can also induce relevant changes (Δ) in the consortium ('community biomass') E (Zhang et al., 2016). This via a proportionality factor '$\eta\gamma$', in mathematical terms (Eq. 1) and graphically (Fig. S1):

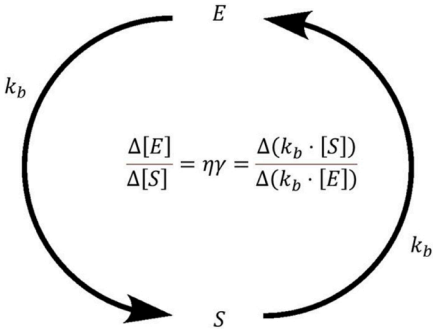

$$\frac{\Delta[E]}{\Delta[S]} = \eta\gamma = \frac{\Delta(k_b \cdot [S])}{\Delta(k_b \cdot [E])} \quad (1)$$

Wherein k_b is a second-order rate constant for production of E (precursors) from consumption of S. The proportionality between acclimation and biodegradation ($\eta\gamma$ in Eq. 1) reflects the effectiveness of biomass production. Unrealistic simplifications of these changes may give rise to 'order-of-magnitude' discrepancies with real-life observations: after (minutes/hours for transcriptional changes) exposure to [S] (mol/L), the 'biomass of the bacterial community' E (e.g., in mol/L) can settle into a new 'steady-state' (Rios-Miguel et al., 2021), rendering the a-priori experimental half-life, $\propto 1/(k_b \cdot [E])$ for S, meaningless (Ahtiainen et al., 2003; Li and McLachlan, 2019; Nyholm, 1991), Eq. 1. Measuring biodegradation of 10.000+ compounds (ECHA, 2020) in different, continuously changing matrices is time and financially constraining, and not a 'true' solution.

Models including such dependence on concentration (i.e., induction, acclimation and community changes) more robustly describe biodegradation in real-life (flexible) scenarios (Poursat et al., 2019). Most models, however, reflect concentration changes by fitting data to e.g. 'logistic kinetics' (i.e., lag-times (Nguyen et al., 2018)) or 3/2 order kinetics, phenomenologically for a limited number of chemicals, concentrations and incubations (Brandt, 2002; Nolte et al., 2018). As a result, limited mechanistic interpretation hampers robust predictions for new situations.

Studying interactions and functions within microbial inocula helps to optimize, interpret and extrapolate experimental findings associated with biodegradation to the community level (Kowalczyk et al., 2015), to predict biodegradation in the field. "Omics" (i.e., transcriptomics, proteomics, interactomics, metabolomics), e.g. via "next-generation sequencing" approaches (Mishra et al., 2020; Rodríguez et al., 2020), opts to link appropriate biomarkers of a (single) culture to biodegradability (Achermann et al., 2020; Kowalczyk et al., 2015; Paniagua-Michel and Olmos-Soto, 2016; Young, 2005). The interplay between (the composition of) microbial consortia and 10.000+ potential substrates is however yet to be captured in a kinetic framework. Ideally, such a framework describes interactions between compounds (De Zwart and Posthuma, 2005; Vrijheid et al., 2016), e.g., mixture effects like co-metabolism. Especially because screening compound libraries (10–1.000 €/sample) extrapolates to high costs (Alves et al., 2018; Balcom et al., 2016; Chai et al., 2018; Johnson et al., 2015). 'Cheap' parameters effectuating acclimation (biomarkers) make best use of omics knowledge and can be implemented to predict kinetics for any substrate. Below, we derive and apply the mechanism-based formulas for such kinetics making use of cheap parameters.

2. Theory

Elevating the concentration of a 'xenobiotic' substance above its value background can, eventually and, under some conditions, induce a higher concentration of biomass enzymatic 'co-factors' $[E_1 \ldots E_x]$. The umbrella term, 'cofactors' refers to all that which constitutes $[E_1 \ldots E_x]$ a contribution to 'growth' (anabolism) by catabolizing the substrate. 1…x include many enzymes, transporters, coenzymes and, indirectly, nucleic acids, lipids and all that which is required to make the cellular biomass function as an expanding self-propelling machinery (see also *Section 3.1.2*). Induction involves a metabolism specific to (a family of) substrates including many biomass forms (1…x) which bind and convert substrates and their intermediate metabolites. Eq. (2) expresses the production of biomass cofactors (i.e., enzymes, transporters, etc. aiding the metabolism) (Monod, 1942; Nolte et al., 2018):

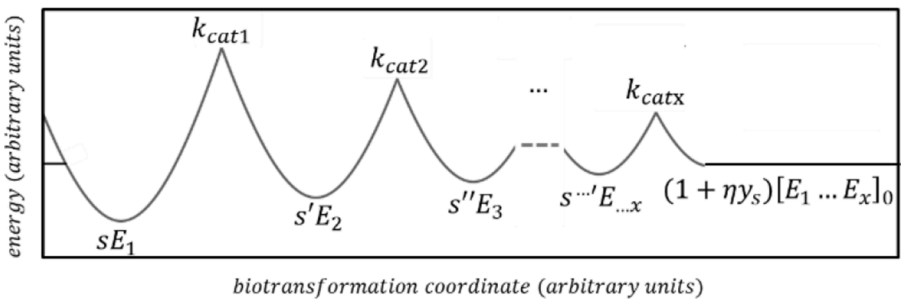

Fig. 1. Simplified illustration of partial energy versus biotransformation coordinate. The horizontal distance between the bottoms of the parabolas represent the (physical) pathway distance between the different enzymes and transporters (steps coupled to process S). Minima of the parabola represent equilibria states of the bonded S-E complexes. Each energy barrier (catalytic transformation) can include both entropy decrease and enthalpy increase. The Figure assumes that the stepwise change in energies is evenly distributed between pathway steps (Astumian, 2019).

$$\begin{aligned}&[S]+[E_1\ldots E_x]_{t=0}\rightarrow^{k_{f1}}_{k_{r1}}[SE_1]+[E_1\ldots E_x]_{\notin E_1}\rightarrow^{k_{cat1}}\\&[S']+[E_1\ldots E_x]_{t=0}\rightarrow^{k_{f2}}_{k_{r2}}[S'E_2]\ +[E_1\ldots E_x]_{\notin E_2}\rightarrow^{k_{cat2}}\\&[S'']+[E_1\ldots E_x]_{t=0}\rightarrow^{k_{f\ldots x}}_{k_{r\ldots x}}[S''E_x]\ +[E_1\ldots E_x]_{\notin E_{\ldots x}}\rightarrow^{k_{cat\ldots x}}\\&(1+\eta y_S)[E_1\ldots E_x]_{t=0}\end{aligned}\tag{2}$$

$k_{f1\ldots x}/k_{r1\ldots x}$ are forward/reverse binding rate constants for the first (1) to the final (x) transporters, carriers and binding domains (in $M^{-1}d^{-1}$ and d^{-1}, resp.). In turn, $k_{cat1\ldots x}$ (in d^{-1}) corresponds to the first (1) to final (x) catalytic steps. Eq. (2) denotes the production of 'new' metabolic cofactors $[E_1\ldots E_x]$ via a number of metabolic steps x, with the net result (yield) being that for every molecule of S consumed, y_S of new cofactors $[E_1\ldots E_x]$ can be produced in addition to initial $[E_1\ldots E_x]_{t=0}$ (net number of biomass cofactors produced from S) (VanBriesen, 2002). y_S is a unitless theoretical (growth) yield efficiency on substrate S normalized by the initial S and biomass concentration, $y_S = y\cdot\frac{[S]_0}{[E_1\cdots E_x]_0}$ (Yuan and VanBriesen, 2002a). In the case of $y_S = 0$, we get empirical 'Michaelis Menten' kinetics, which constitutes a mix between first and second order kinetics; $y_S > 0$ can lead to 'mixed Monod' or Michaelis–Menten–Monod (MMM) kinetics (Brandt, 2002; Maggi and la Cecilia, 2016). $\eta_{q1\ldots x}$ is an umbrella term for effectiveness of the biomass (and production thereof). $\eta_{q1\ldots x}$ accounts for cases that transformation of S (or subsequent S', S'', etc.) does not contribute to cofactor E production (e.g., non-growth co-metabolism (Dalton and Stirling, 1982; Luo et al., 2014)): when endemic metabolism is completely ineffective in converting S to E, $\eta_{q1\ldots x} = 0$. See Fig. 1.

Eq. 2 and Fig. 1 are abstract versions of reality: the rate of every step (1…x) depends on (co-)substrate, intermediates, reaction product, energizing molecules such as ATP and other coenzymes/cofactors and regulators. Thus, processes in Eq. 2 come on top of existing metabolism ($[E]_{t=0}$ normalized to 1 in Eq. (2)), i.e., maintenance when organisms are in a stationary growth state (zero net growth). The concentration of biomass cofactors, i.e., $[E_1\ldots E_x]$, can change over time: induction may occur via (exponential) 'growth' of new pathways, existing pathways, or inhibiting them (negative y) (Chong et al., 2010, 2011). A general equation capturing changes in concentration of effective biomass is:

$$\begin{aligned}\eta_{q,1\ldots x}[E_1\ldots E_x]_t\ &=\eta_{q1\ldots x}\cdot[E_1\ldots E_x]_0-\int_{\tau=0}^{\tau=t}\eta_{1\ldots x}\cdot y_S\cdot\frac{d[S]}{d\tau}\cdot d\tau\\&=\eta_{q1\ldots x}\cdot\left([E_1\ldots E_x]_0+y_{S,1\ldots x}\cdot([S_0]-[S])\right)\end{aligned}\tag{3}$$

neglecting any (short-term) dependence of the steady-state (maintenance) metabolism on substrate concentration. The substrate decreases with time in proportion to both biomass and substrate concentration:

$$\frac{d[S]}{dt}=-k_b\cdot\left|\eta_{q1\ldots x}\cdot[E_1\ldots E_x]_0+y_S\cdot([S_0]-[S])\right|\cdot|[S]|\tag{4}$$

wherein k_b is a second order biodegradation rate constant (Nolte et al., 2020c), which defines the rate constant k as:

$$k\overset{\text{def}}{=}(1+y_S)\cdot\eta_{q1\ldots x}\cdot[E_1\ldots E_x]_0\cdot k_b\tag{5}$$

which is the apparent (maximal) attainable 'first-order' rate constant when S is 100% biodegradable (when the non-biodegradable $[S_{NB}] = 0$) (Quiroga, 1994). When S is partially degradable ($[S_{NB}] > 0$ and constant) Eq. (4) simplifies to a Haldane differential equation (Brandt, 2002; Haldane, 1930; Quiroga et al., 1999; Romero, 1991). One can obtain a specific solution to Haldane (details in SI) expressing half-life as:

$$t_{1/2}=\frac{ln\left(2+\eta_{q1\ldots x}\cdot\frac{y_S\cdot[S_0]}{[E_1\ldots E_x]_0}\right)}{k_b\cdot\eta_{q1\ldots x}\cdot\left([E_1\ldots E_x]_0+y_S\cdot[S_0]\right)}\tag{6}$$

For low initial effective biomass ηE_0 and high y_S, the decrease in [S] is very small at first (i.e., a lag-time (Swinnen et al., 2004)), then only increases to mono-exponential at low substrate concentration.

2.1. Low concentration and steady-state limit

Xenobiotics usually have no/few dedicated, specific transporters or metabolic pathways. By analogy, the horizontal distances between the bottoms of the parabolas in Fig. 1 are infinite/large. As minority ligands, xenobiotic S can then be 'moonlighting' on transport systems and pathways (enzymes), 'in use' by other substrates, bestowing them with apparent first-order kinetics. In absence of 'natural' substrates, xenobiotics can become majority ligands, though, 'micropollutants' (pharmaceuticals; pesticides) exist in environments in <1 μg/L, rarely saturating transporters or enzymes ($[E_1]>>>[SE_1]$). In such limits, the k_b ($M^{-1}s^{-1}$) is (Astumian, 2019; Canela et al., 2019; Nolte et al., 2020c):

$$k_b=\frac{k_{f1}\cdot k_{cat1}}{k_{r1}+k_{cat1}}=\frac{k_{cat1}}{K_{M1}}\tag{7}$$

capturing both transport and catalysis; when reactant and transition state are in rapid equilibrium, K_m (concentration of S at half maximal velocity) equals the affinity constant K_d (Nazzal, 2016). Natural substances (amino acids, sugars, etc.) are ancient and more ubiquitous (e.g., in WWTPs $[S]>1$ μg/L (Yang et al., 2020)). Hence, microbes will have evolved [E] with higher affinities (k_{f1}, k_{f2} … k_{fx}). This lets microbes achieve a larger amount of molecules at active sites (transporters, enzymes), $[SE]$, hence, higher turnover for natural (growth) substrates (Hardin et al., 2009). On this basis, organisms will have (quickly) consumed (1) and processed (…x) S until they reach 'steady-state' with 'stationary growth' (e.g., wherein $[S] < 1$ μg/L), so that the simplification above can again apply.

2.2. Experimental yield effectivity

For high initial effective biomass ηE, relative to S (which in the range of μg/L) and/or low yield ($y\rightarrow 0$), bacterial consortia remain in steady-state. We then expect mono-exponential decrease/decay in the concentration of S to that of the non-degradable part (i.e., no lag times). In case the yield and $[S]_0$ are low as compared to initial biomass Eq. (6) reduces to:

$$t_{1/2}=\frac{ln(2)}{k_b\cdot\eta_{q1\ldots x}\cdot\left([E_1\ldots E_x]_0+y_S\cdot[S]_0\right)}\tag{8–1}$$

k_b is known from previous SBR studies (Nolte et al., 2020c; Nolte and Ragas, 2017). Also, (experimental) biomass $\eta_{q1\ldots x}\cdot[E_1\ldots E_x]_0$ is often (kept) fairly constant or in (pseudo) steady-state because of low (e.g., <μg/L) xenobiotic concentration, implying negligible toxicity. This opens the door for facile calculation of the effective biomass yield ($\eta_{q1\ldots x}\cdot y_S$) from information on concentration and degradation, Eq. 8. Experimental data (surface waters; wastewaters) on half-lives $t_{1/2}$ and k_b (Eq. 8) will expose values for $\eta_{q1\ldots x}\cdot y_S$ representing concentration-dependency, i.e., effective yield from xenobiotics in 'real-life' diverse environments.

$$\Delta\left(\eta_{q1\ldots x}\cdot y_S\right)\approx\frac{ln(2)}{t_{1/2}\cdot k_b}\tag{8–2}$$

Having such experimental values for $\eta_{q1\ldots x}$ enables (corr)relating them to other variables; constituting a basis for interpretation to enable its prediction.

2.3. Predicting yield effectivity

Binding to (enzyme's) active sites (k_f, k_r) enable catalytic steps (k_{cat}) to take place (Eq. 2;7). Thus, capturing yield involves acknowledging binding (i.e., transport) and catalysis. Within a 'common' metabolism (enzymatic steps), i.e. $\Delta\eta_q$=0, an observed ηy reflects the stoichiometric (theoretical) yield ('maximum efficiency') and in turn, thermochemistry (McCarty, 2007; VanBriesen, 2001; Yuan and VanBriesen, 2002a). The elemental composition of substrate S determines the stoichiometry of

reactions, which differs between substrates. This, however does not take into account the effectiveness η_q of the biomass E (production). A priori, $\eta_{q1\ldots x}$ denotes effectiveness of the biomass (production) from S, reflecting transport, connectivity/coupling, transcription (speed), etc.; $\eta_{q1\ldots x}$ can take the form of a matrix function (Astumian, 2019; Ferraz de Arruda et al., 2018; Lee et al., 2006).

Microbes usually incorporate/channel xenobiotic S into (operationally) 'efficient' primary metabolic structures/pathways. They transform (couple) a xenobiotic (in)to a compound that plays a (more) central role in metabolism (Westerhoff et al., 1982). Therefore, pathways overlap (i.e., are partially in common) and the observed biodegradation (i.e., $\eta_{q1\ldots x}$) will represent a weighed 'distance' for multiple of such central metabolites (e.g., carbohydrates in the Krebs cycle). Substrate S and, by extension its metabolites (S', etc.) induce (the production of) cofactors. No biochemical reaction is 100% efficient though and for every metabolic step (in common) there will be a definite (Gibbs) energy dissipation (Astumian, 2019; Trapp et al., 2018; VanBriesen, 2002; Westerhoff and van Dam, 1987). When the number of 'required' metabolic steps (needing 'maintenance') increases, the production of $E_{1\ldots x}$ from S will be less effective. In other words, if the metabolic pathway is long, energy 'loss' accumulates along each step so that a lower effective yield $\eta_{q1\ldots x}{\cdot}y$ can be achieved (McCarty, 2007). Fig. 2 envisions stoichiometries to reflect path functions in thermodynamic quantities (Chen et al., 2017): effective (green) and 'non-effective' (gray) pathways.

We hypothesized that $\eta_{q1\ldots x}{\cdot}y_S$ can be captured (predicted) by combining elemental compositions of substrates S with those of biomass cofactors $E_{1\ldots x}$. The combination of stoichiometries of biochemical reactions then (co-)determines the effectivity of metabolic pathways: stoichiometric (molar) ratios 'ν' reflect projections of η on y. We set out to connect compositions of S to those of $E_{1\ldots x}$ by calculating values for stoichiometric ratios ν_s, combining and comparing them with experimental values of $\eta_{q1\ldots x}{\cdot}y_S$. Comparison yielded statistically significant relationships signifying relevance of $\eta_{q1\ldots x}{\cdot}y_S$ in multiple environments. The resulting predictions are biochemically intuitive and can supplement SBR and kinetic fate models.

3. Methods

We considered the production y_s of effective metabolic biomass 'machinery' ηE (*Section 2.2*) from any substrate S_i, and co-substrates x_i. The y_s corresponds to the theoretical (maximal) yield of the machinery produced when substrate S is added to medium. We determined an experimental effective yield $\eta{\cdot}y_s$ and an apparent stoichiometric ratio ν_s: the first one is experimentally derived, the second one is predicted. We then compared and contrasted the two.

We predicted values for $\nu_{s,i}$ on the basis of stoichiometric solutions of the generalized reaction equation (details in *Section 3.1*):

$$\nu_{s,i} \in s_i[S] + x_i[\mathrm{X}] \rightarrow e_i[E_i] \tag{9}$$

With s_i, x_i and e_i the numbers of elements within (the concentrations, in square brackets of) S, X and E. In view of the richness of microbial biochemistry, we assumed that all these reactions are possible (i.e. $x{=}\infty$ and in other words, $[S_{NB}]_{t\rightarrow\infty}{=}0$ (Ouiroga et al., 1999), Eq. (5), or coupling $q{\neq}0$ (Westerhoff et al., 1982)), though at different rates. We took the rates of reactions to be proportionally higher with higher yields (i.e., lower Gibbs energy dissipation). We combined the individual contributions $\nu_{s,i}$ to predict the 'apparent' stoichiometric ratio by treating them as resistances (of flows) through each metabolic chain (Westerhoff et al., 1982) which are connected in parallel (*Section 3.1.3*):

$$\nu_s \propto \left(\sum_1^i \frac{1}{\nu_{s,i}} \right)^{-1} \tag{10}$$

We evaluated the relevancy of predictions of ν_s by comparison with 'experimental' values for $\eta{\cdot}y_s$: considering the rate constant and exponential decay in Equation 8, we calculated experimental values for $\eta{\cdot}y_s$ via:

$$\Delta\left(\eta{\cdot}y_{s,\ exp}\right) = \frac{k}{k_b} \tag{11}$$

Wherein k is the observed first-order biodegradation rate constant in surface-/wastewater. We obtained values for k from an empirical QSBR

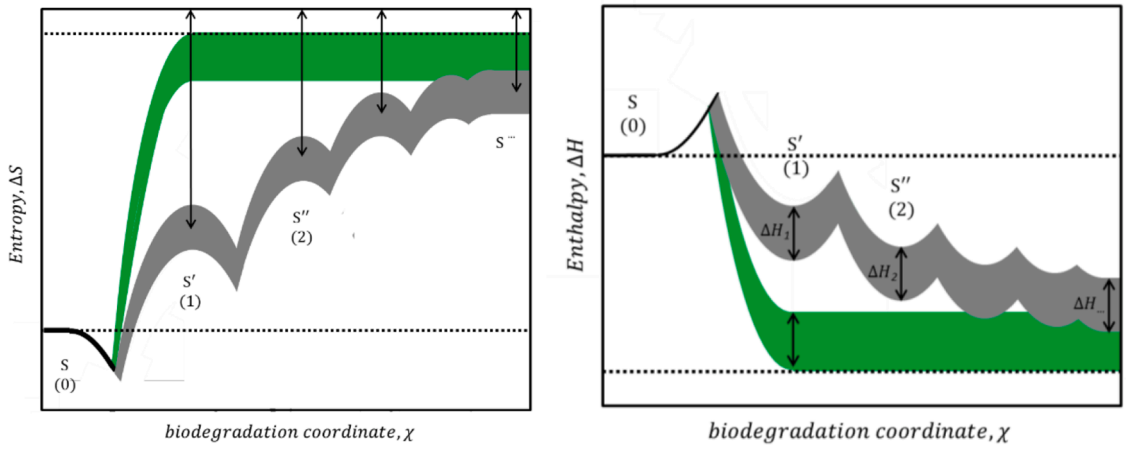

Fig. 2. Illustration of total standard entropy (A) and enthalpy (B) changing along the biodegradation coordinate (aggrupation of distances between molecules/atoms of substrates, metabolites and cofactors). The green band shows an 'efficient' metabolic pathway (high ηy), contrasting with the gray band (low ηy). Further into the coordinate, the energy barriers become smaller, and thus the rate constants become larger. Acknowledging that there may be multiple reaction paths as influenced by substituents and not every chemical bond is energetically identical, energies are depicted as bands rather than lines. A: The gray band shows how the standard entropy changes as the substrate moves along the reaction coordinate through an entire metabolic pathway. It begins with a black segment representing (on the far left) the equilibrated state of the parent substrate. Following the band to the right shows a decrease in entropy of the activated state, i.e. the smaller number of substrate states from which the substrate is ready to react to the product of the first reaction, i.e. metabolite 1 (i.e. S'). As the molecule moves to the larger number of equilibrated states of metabolite 1, its entropy increases. The states of metabolites S', S'', etc. are (arbitrarily) shown to have higher entropy than that of the original substrate *s*, also because the substrate is being converted into additional 'biomass' $y_s[E_1\ldots E_x]_0$, which is of greater complexity (Sousa et al., 2006). The arrows represent the potential entropy increase from metabolizing S. B: The standard enthalpy of the substrate substance as it passes down the metabolic pathway, running through activated states in between these. The green band shows an 'efficient' metabolic pathway, contrasting with the gray band. The intersections between parabola (maxima) denote bond breaking/formation between elements, i.e., activation enthalpies.

(Nolte et al., 2020c, 2018), EpiSuite's BIOWIN and other datasets (see *Section 3.2.1*). We calculated k_b by applying aspects on diffusion, steric hindrance and energetics (Eyring) (Nolte et al., 2020c) (*3.2.2*). Variance from the $[E_1 \ldots E_x]_0$ term was accounted for via data curation (*3.2.1*).

3.1. Prediction of ν_S

3.1.1. Stoichiometry

We predict contributions to ν_S via of the 'pollutant' S to those of biomass cofactors E (Eq. (12)). We do this by solving algebraically stoichiometric equations for each (i) E_i:

$$\begin{Bmatrix} (p_S + p_{x,i})[\boldsymbol{P}] \\ +\,(c_S + c_{x,i})[\boldsymbol{C}] \\ +\,(h_S + h_{x,i})[\boldsymbol{H}] \\ +\,(o_S + o_{x,i})[\boldsymbol{O}] \\ +\,(n_S + n_{x,i})[\boldsymbol{N}] \\ +\,(s_S + s_{x,i})[\boldsymbol{S}] \end{Bmatrix} \rightarrow^{k_{cat1\ldots x}} \begin{Bmatrix} (p_{E,i})[\boldsymbol{P}] \\ +(c_{E,i})[\boldsymbol{C}] \\ +(h_{E,i})[\boldsymbol{H}] \\ +(o_{E,i})[\boldsymbol{O}] \\ +(n_{E,i})[\boldsymbol{N}] \\ +(s_{E,i})[\boldsymbol{S}] \end{Bmatrix} \quad (12)$$

Wherein $p_S \ldots s_S$ are the element concentrations (elements in bold capital letters), in number per substrate molecule S for each reaction. Likewise, the decapitalized letters $p_x \ldots s_x$ are the number concentrations of co-substrates. Co-substrates are needed because the stoichiometric ratios in substrate and cofactor E_i may not match up. The entries $p_E \ldots s_E$ are the element number concentrations of the biomass cofactors. We obtained the elemental compositions via solving the stoichiometry equation, Eq. 12, via applying the argument:

$$\underset{\rightarrow 0}{min}\left(CV\left| \frac{n_{x,i}+n_s}{n_{E,i}}, \frac{h_{x,i}+h_s}{h_{E,i}}, \frac{s_{x,i}+s_s}{s_{E,i}}, \frac{p_{x,i}+p_s}{p_{E,i}}, \frac{o_{x,i}+o_s}{o_{E,i}}, \frac{c_{x,i}+c_s}{c_{E,i}} \right| \right) \quad (13)$$

which minimalizes the difference between elemental ratios before and after the reaction (Eq. 12), via their coefficient of variation, CV. In other words, the argument (Eq. (13)) solves equation 12 for each i. The required accuracy of the stoichiometric solution, in terms of the CV of the ratios (Eq. (13)), was set at $\leq 1 \times 10^{-4}$. Based on equation 12, we define the contributions to ν_s as:

$$\frac{1}{\nu_{s,i}} = 1 - \frac{\sum n_x, h_x, s_x, p_x, o_x, c_x}{\sum (n_x + n_s), (h_x + h_s), (s_x + s_s), (p_x + p_s), (o_x + o_s), (c_x + c_s)} \quad (14)$$

Outcomes of 1 and 0 for $\nu_{s,i}$ denote that, respectively, no and an infinite number of co-factors X are needed to produce *i*. With *i* being hypothetical constituents of biomass cofactors, as defined below.

3.1.2. Stoichiometric parameters

The elemental compositions of biomass cofactors differ. We therefore determined the individual (i) contributions to ν_s (Eq. (14)) via biomass-specific stoichiometries. However, virtually endless biomass cofactors i can be involved (enzymes, transporters, coenzymes, nucleic acids, lipids, etc.). Keeping the parametrization to a minimum, we broadly distinguished between 4 important metabolic routes: lipid, amino acid, carbohydrate and nucleic acid metabolism (Hendriks et al. 2016; van Lier J. B. et al., 2008; Yang et al., 2020). An additional 5th term acknowledges 'general' or 'background' metabolism involving 'hybrid'/-multifunctional enzymes, transporters, etc. (Table 1). Thus, we simplified *i* to be 5. We took the elemental ratios of 'background metabolism' from (Fagerbakke et al., 1996; Popovic, 2019; Vrede et al., 2002), and specifically included phosphorous as a characteristic of life (Hunter, 2012; Kamerlin et al., 2013).

3.1.3. Metabolic routes, i

Microbes may prefer a particular metabolic route over another: the colored lines in Fig. 3 signal particular routes which S may follow. We conveniently choose the potential metabolic routes to be lipid, amino acid, carbohydrate, nucleic acid and background metabolism (as in *3.1.2*). Naturally, the observed metabolism will likely occur via the fastest available and most effective route (González-Cabaleiro et al., 2015), the 'path of lowest resistance' (Chen et al., 2017), e.g. green instead of gray in Fig. 2. We consider the main metabolic routes to function in parallel, treating them as resistances (Eq. (15)) (Westerhoff et al., 1982), as shown graphically in Fig. 3:

$$\frac{1}{\nu_s} = \frac{1}{\nu_{s\,i=carbohydrates}} + \frac{1}{\nu_{s\,i=aminoacid}} + \frac{1}{\nu_{s\,i=nucleicacid}} + \frac{1}{\nu_{s\,i=general\ background}} + \frac{1}{\nu_{s\,i=lipid}} \quad (15)$$

Thereby, we implement Eq. (15) (with $i = 5$) as the calculation of the 'metabolic resistance' of *s* according to equation 21, wherein i represents the biomass cofactor constituent. A more thorough interpretation of the values for ν_s thus obtained is given in the discussion. The values are a measure for 'biological likeness' (Fig. S1) or 'natural' character of the substrate (Table 2).

3.2. Experimental $\eta \cdot y_s$

3.2.1. Data

We considered three independent datasets for *k* to calculate 'experimental' values for $\eta \cdot y_s$. The first is the EpiSuite dataset to develop BIOWIN (Ver 4.0) (giving scores between 0 and 5 for biodegradability in wastewater) (USEPA, 2012); we assume that $a \pm 1$ difference in the BIOWIN score translates to an order of magnitude in *k*. The second, for surface water, is an in-house dataset (Nolte et al., 2020c) containing electron-rich substances and carboxylates. A third data subset of *k* values was on nitrogen-containing substances (Evenblij et al., 2020).

To allow comparing results from datasets, we aligned the EpiSuite dataset to the in-house dataset. Specifically, we excluded carboxylic acids esters from the EpiSuite dataset because of potential abiotic hydrolysis, whereby values of DT_{50} were all below 100 days for pH>8 and <6 in environmental aqueous media. We also excluded EpiSuite data for salts containing (toxic) metal (e.g., Zn, Al) ions. We further excluded compounds for which the octanol-water partitioning ratio ($^{10}\log(K_{OW})$ exceeded 4, to minimize potential convoluting influence of (non-linear) sorption (Nolte et al., 2018; UnitedNations, 2011).

3.2.2. Calculation of experimental $\eta \cdot y_s$

Biodegradation of structurally diverse micropollutant adheres to 2nd order kinetics (Paris et al., 1981), but data for *k* represents pseudo 1st order kinetics because low (micropollutant) concentrations (data curation) render the effective biomass $\eta \cdot E$ (in surface- and waste water) constant (via steady state). We take k_b in Eq. (11) to be a product function (Nazzal, 2016; Nolte et al., 2020c). We thus acquire 'experimental' values for $\eta \cdot y_s$ by plugging in values for *k* and k_b (*P* and *A*):

$$\Delta(\eta \cdot y_s) = \frac{k}{P \cdot A \cdot e^{\Delta G^{\ddagger}}} \quad (16)$$

Wherein *P* is a partitioning function (Bar-Even et al., 2011; Pirovano et al., 2014) (taken as $P \sim 0.09 \cdot K_{OW}$, with K_{OW} at pH~7.4 (Nolte et al., 2020c)). In the presence of electrolyte, carboxylates can bind biomass via ion exchange rather than hydrophobic interaction: thus, we calculated *P* in Eq. (16) for positive charges attached to the carboxylates. *A* is a 'frequency' factor (calculation details in (Hill, 1976; Nolte et al., 2020c)) and $e^{\Delta G^{\ddagger}}$ is the thermodynamic reaction efficiency (Eyring, 1935; Nazzal, 2016) from chemoinformatic calculation. Fig. 4 visualizes the calculation of experimental $\eta \cdot y_s$. By applying Eq (16), we calculated $\eta \cdot y_s$ by correcting the data on *k* for *A* and $\Delta G^{\ddagger}$. Then, the difference in $\eta \cdot y_s$

Table 1
Elemental composition of major biomolecule groups, taken from previous reports (Hendriks et al. 2016; Fagerbakke et al., 1996; Popovic, 2019; Vrede et al., 2002). * values represent a generic composition of bacteria.

Biomass cofactor i	Nitrogen, $n_{E,i}$	Hydrogen $h_{E,i}$	Sulfur $s_{E,i}$	Phosphor. $p_{E,i}$	Oxygen $o_{E,i}$	Carbon $c_{E,i}$
BACKGROUND*	0.15	2	0.05	0.05	0.5	1
LIPID	0.6	79.2	0	1	8.8	41
CARBOHYDRATE	0	12	0	0	6	6
AMINO ACID	1.45	9.85	0.1	0	2.45	5.35
NUCLEIC ACID	3.4	14	0	1	8	9.6

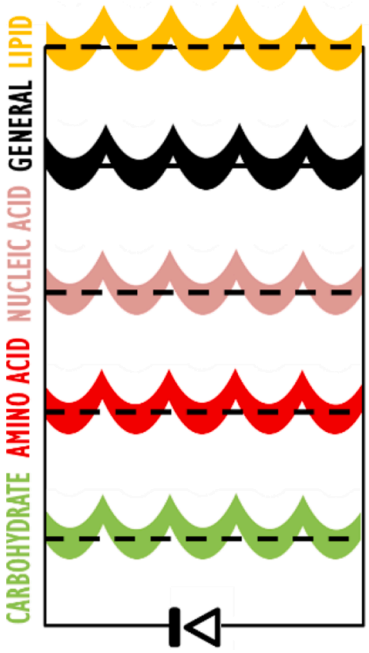

Fig. 3. Schematic of metabolic cycling of four major biomolecules. Colors illustrate metabolic routes that a cell or substrate may 'prefer'.

between substrates becomes visible:

We need activation energies $\Delta G^{\ddagger}$ as they influence biodegradation (Nolte et al., 2020a, 2020c; Rorije et al., 1995), Eq. (16). Calculating $\Delta G^{\ddagger}$ for, potentially, 10.000+ substrates and enzymes is cumbersome and sometimes error-prone (ECHA, 2020; Jaladanki et al., 2020). Hence, we minimized the influence of $\Delta G^{\ddagger}$ (hence, error) by considering electron-rich (electrochemically neutral) substrates S separately, such that there is negligible variation in $\Delta G^{\ddagger}$ values between S: $\Delta_S(\Delta G^{\ddagger}) \approx 0$ (Nolte et al., 2020c). In the case of carboxylates and nitrogen as heteroatoms, the term $\Delta_S(\Delta G^{\ddagger})$ could not be ignored; we applied the assumption of LFER (Jinich et al., 2018; Nolte et al., 2020c):

$$\Delta_S(\Delta G^{\ddagger}) = F_c \cdot \sigma \cdot \Delta_S(\Delta G_r + \Delta G_{ct}) \quad (17)$$

Assuming transformations are overall oxidative, we calculated $\eta \cdot y_S$ for carboxylates (taking $\Delta G_{CT}=0$) and nitrogen-containing substrates ($\Delta G_{ct}>0$) via (Karki and Dinnocenzo, 1995; Nolte, 2020b; Nolte et al., 2020c). We assumed that the 'reacting atom' is well defined (Rudik et al., 2016): the orbital density overlap (F_c term) is a constant factor for all S, $\Delta F_c = 0$ (Nolte et al., 2021).

3.3. Testing

The apparent yield effectivity, $\eta \cdot y_s$ is a complex quantity. We therefore cannot evaluate its absolute accuracy, but can do this merely in abstract terms by inferring plausibility of our calculus. We evaluate the accuracy of the prediction of $\eta \cdot y_s$ via calculated values from three different datasets (*Section 3.2.1*). Allowing comparison with widely applied statistical methods, we chose to calculate p-values to evaluate significance and the Pearson's squared correlation coefficient (R^2) to evaluate preciseness. The values for $\log(k_b)$ and $\log(k)$ (standard errors of 0.5–1.0 (Nolte et al., 2020c), in log-scales) entail uncertainty and variability (resp.), partially due to unknown involvement of E_i, which propagate into errors in the 'experimental' $\eta \cdot y_S$ (e.g., maximum R^2 obtainable for a perfect model is ≈0.3). To evaluate prediction errors, we thus compared errors in 'experimental' $\eta \cdot y_S$ to its discrepancy with predicted ν_S.

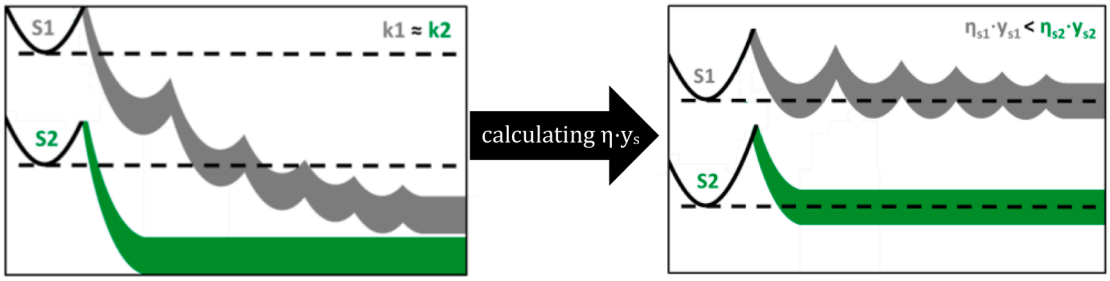

Fig. 4. Energy diagram and biodegradation coordinate according to k, as function of $\eta \cdot y_s$, A and $\Delta G^{\ddagger}$. The standard chemical potential (enthalpy) of the substance decreases along the pathway. Arrow denotes correcting data on k for A and $\Delta G^{\ddagger}$ to calculate 'experimental' $\eta \cdot y_s$. The gray/green curves illustrate energetics along the metabolic chain.

4. Results

4.1. Experimental values for $\eta \cdot y_s$

We calculated 'experimental' values for the effective E yield $\eta \cdot y_s$. The values reflect the concentration dependency in Eq. 1 (and Fig. S1). The values for $\eta \cdot y_s$ largely vary by 3 orders of magnitude between substrates, i.e., $\Delta(\eta \cdot y_s) = 1000$ (Figs. 5;6, vertical axes). For data subsets, variation is larger (Figs. 6;7). The compounds we generally consider as being 'natural', 'biological' and 'organic' compounds show high values for $\eta \cdot y_s$, implying that these chemicals are relatively easily biodegradable. We note that uncertainties values for experimental $\eta \cdot y_S$ are approximately 1 order of magnitude, stemming largely from the uncertainties in the raw data on k. Uncertainties were larger as compared to variance in v_S, more so for specific chemical classes.

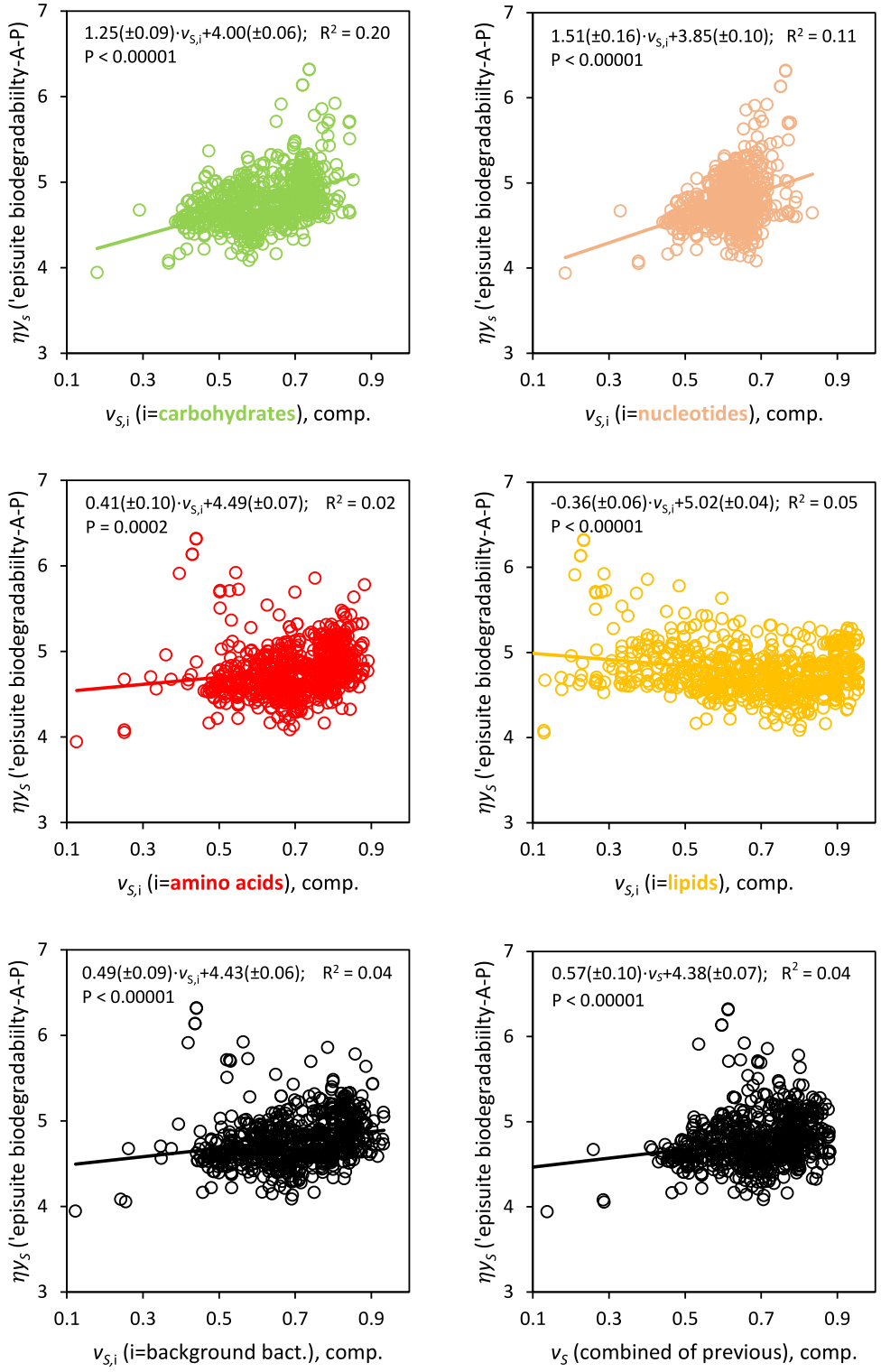

Fig 5. ηy_S as calculated from experimental biodegradation (EpiSuite) data (y-axes, in ^{10}log-scale) versus v_S as computed using Equations 18–21. Colors correspond to metabolism.

4.2. Predicted values for $v_{s,i}$ and v_s

Implementing the values in Table 1 as parameters in Eqs. 12-15 yielded apparent stoichiometric ratios $v_{s,i}$ *and* v_s (predicted concentration dependencies), Table 2. Combining the metabolic paths v_{si} by treating them as resistances (Eq. 10;15), gave v_s values varying mostly between 0.4–0.9 (Figs. 5–7). By illustration, a bacterial consortium will find it virtually impossible (to adapt) to efficiently degrade sulfur hexafluoride and fullerene unless *many* other co-substrates X are available. In contrast, most consortia will already have machinery to use e.g., fatty- and amino acids. For instance, gabapentin (a γ-amino acid), has high v_s (asterisk in Fig. 7).

4.3. Metabolic paths i

Analysis yielded statistically significant correlation ($p<0.05$) between $\eta \cdot y_S$ and all individual contributions from v_S (i.e. $v_{S,i}$) for specific metabolism (i), Fig. 5A-E. This was true for EpiSuite data, but using our in-house data only the contributions (i) from carbohydrates, nucleotides (Fig. 6A;Fig. 6B;Fig. 7A) and amino acids (Fig. 7C) appeared significant. We did however observe a significant correlation for carboxylates as a specific chemical class (filled vs. open data points, Fig. 6C;D).

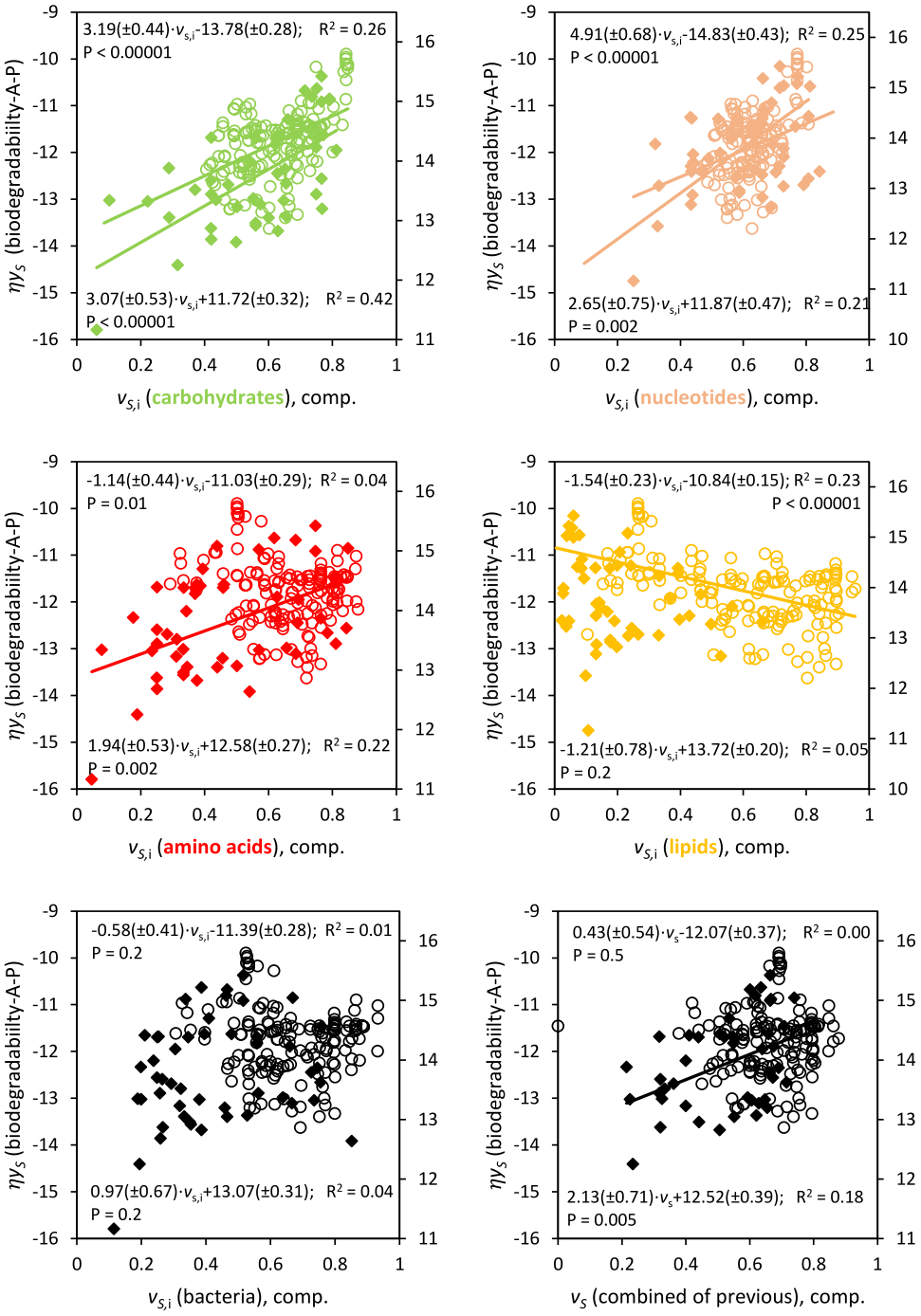

Fig. 6. Experimental ηy_S (from Nolte et al. 2020 data), y-axes, versus computed v_S (Eqs. 12–15), x-values. Circles are compounds with exclusively C, O or H atoms (left y-axis, ^{10}log-scale); filled diamonds are carboxylates (right y-axis, log-scale). Solid lines denote statistically significant correlations. Top/bottom equations refer to all compounds, and carboxylates, resp. Colors correspond to metabolism.

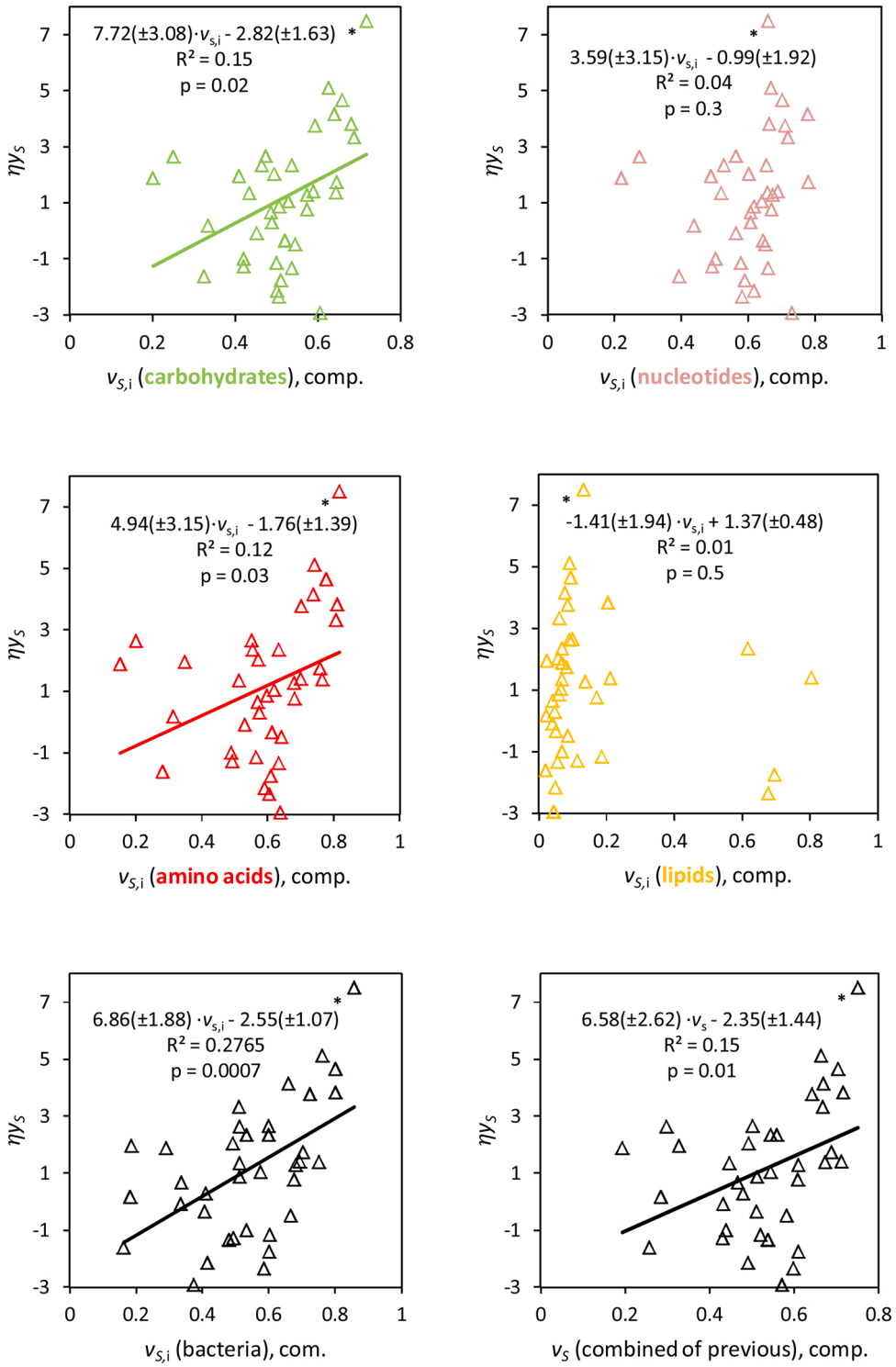

Fig. 7. Experimental ηy_S as calculated from experimental removal efficiency (WDOD) data, y-axes, versus computed v_S (Eqs. 12–15), x-values. Green triangles are compounds with nitrogen. Gabapentin (γ-amino acid) is marked with *. Solid lines are statistically significant correlations. Colors correspond to metabolism.

Envisioning C—N cleavage metabolism (Nolte et al., 2020a), preliminary investigations on N-rich compounds (excluding other heteroatoms) did not yield statistically significant relationships between experimental $\eta \cdot y_S$ and any predicted v_{Si}, including nucleotide- and amino acid metabolism (i). This was with exception of the homogeneous WDOD data (significant relationships in Fig. 7).

All contributions (i) from $v_{S,i}$ to $\eta \cdot y_S$ were positive, i.e., correlations yielded $R>0$. This was with exception of v_{Si} for which we took $i=$ lipid cofactors (Fig. 5D-7D, i.e., $R<0$), discussed in Section 4.3. The slopes of the regressions were highest when taking $i=1=$ carbohydrate and when taking $i=1=$ nucleotide cofactors (Fig. 5,6). Slopes differed slightly for E_i as nucleotide cofactors, e.g., in the case when S are carboxylates (Fig. 6B). Since the units of biodegradation (e.g., EpiSuite) differ between datasets, we cannot compare slopes between datasets. However, within for example Fig. 6, biodegradability (in terms of yield effectivity ηy) increases stoichiometrically by 3.2(±0.4) or 3.1(±0.5) via likeness to carbohydrate. This shows that, under steady state acclimation, a compound stoichiometrically identical to carbohydrate (e.g.,

Table 2
Predicted values for v_s according to Eqs. 12-15 and Table 1. Colors illustrate the size of v_s.

Substrate S	elemental composition	v_s
stearate	C18H35O2	0.9
sucrose; glutamine	C12H22O11; C5H10N2O3	0.7
acetaminophen	C8H9NO2	0.6
benzanthracene	C18H12	0.5
carbamazepine	C15H12N2O	0.4
PFOA; ammonium; fullerene	C8F15O2; NH4; C60	0.3
sulfur hexafluoride	SF6	0.0

sugars), will be $10^{3.2(\pm 0.4)}$ or $10^{3.1(\pm 0.5)}$ times faster degraded than a compound marginally similar to carbohydrate. When correlations were statistically significant, the signs of the correlations did not differ between datasets (Fig. 5 compared to Fig. 6; Fig. 7).

4.4. Total metabolism

Comparisons between predicted v_S and experimental $\eta{\cdot}y_S$ are depicted in Fig. 5F;6F;7F (Nolte et al., 2020c). Comparison between v_s (as combined from v_{si}, Eq. 10;15) also yielded a statistically significant correlation with $\eta{\cdot}y_S$ (Figs. 5F; 6F; 7F), prominently for EpiSuite data (Fig. 5F). Taken together, evaluation using data on k from EpiSuite (Fig. 5) led to slightly stronger relationships between predicted v_S and experimental $\eta{\cdot}y_S$, as compared to in-house data for surface water (Fig. 6) and wastewater (Fig. 7). While the involvement of metabolic cofactors i were not weighted (Eq, 15 denotes equal contribution), an analysis excluding general background and lipid cofactors, gave better results. This was with the exception of N-rich compounds (Fig. 7). If the relevance of metabolic cofactors was weighted (e.g., optimizing the numerators in Eq. (15)), this would have yielded a 'maximum' correlation ($R^2 \approx 0.2$–0.3). Multiple analyses show that approximately 90% of the experimental $\eta{\cdot}y_S$ (y-axes) values fall within 1 order of magnitude of the expected value based on v_S (Figs. 5–7). Our corresponding values for v_S (x-axes) vary mostly (~90%) by 0.5. Figs. 5F–7F show that a factor of 0.5 can correspond to a predicted increase in the value of $\eta{\cdot}y_s$ by a factor of ~10^3. A variation of ~0.2 in v_S (x-axes in Fig. 7F), results in a factor ~4 difference in the value of k.

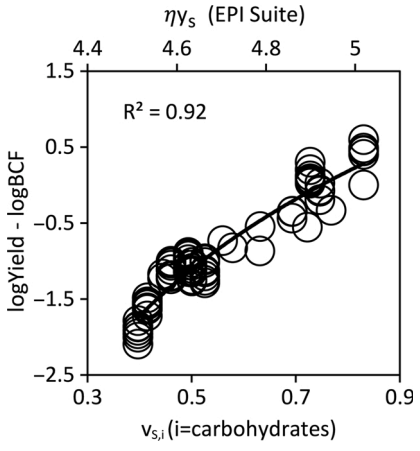

Fig. 8. Yield and bioconcentration in aerobic mixed bacterial cultures of organic compounds (y), versus this study's result (x). Data (y) from literature (Smeaton and Van Cappellen, 2018; VanBriesen, 2002; Yuan and VanBriesen, 2002).

5. Discussion

5.1. Stoichiometry

Microorganisms are vital components of biogeochemical cycles of elements (Filipiak et al., 2017; Luo, 2017; Mishra et al., 2020). Stoichiometry can determine the number of cofactors microorganisms 'need' to degrade S. Equations 12-15 thus solve for stoichiometry, yielding for NH_3 $v_S = 0.0$–0.3 (unitless, based on elemental concentration), depending on cofactors and enzymatic machinery. In comparison, converting 1 mole of NH_3 to biomass requires co-nutrients with N, O and C to increase the biomass by 0.066 mole (i.e., $\eta{\cdot}y \approx 0.1$) (Strous et al., 1998). Cell yields vary with 0.47–0.79 g cells / g BOD (Lim et al., 2001), similar to our variability of 0.4–0.9 (Figs. 5-7). 1 gram of styrene gives 0.675 gs ($\eta{\cdot}y \approx 0.7$) of biomass (Gaszczak et al., 2012), whereas we predicted v_S for styrene to be 0.5–0.7 depending on pathway i. The stoichiometric approach could break down for molecules more complex than NH_3 and styrene. Whereas inorganic substrates (e.g. HPO_4^{2-}; NH_4^+) cycle extensively between biota and environments, natural environments contain only few unique natural molecules that are both abundant (e.g., [S]>1 μg/L) and structurally complex. We find statistically significant predictions for complex and heterogeneous molecules (Figs. 5–7). Among 9 micropollutants, acetaminophen ($v_S = 0.6$) and metoprolol ($v_S = 0.7$) degraded faster than expected based on thermochemistry (Nolte et al., 2020c; van Bergen et al., 2020). To our knowledge, there is no study uniformly evaluating 100+ compounds for fate assessment comparable to ours. We therefore compared to similar data on bioconcentration and aerobic bacterial yield by Yuan and vanBriesen (2002), vanBriesen (2002) and Smeaton (2018), Fig. 8. The combined agreement indicates that stoichiometry describes $\eta{\cdot}y$, i.e., the state of acclimation (Brandt, 2002; Strous et al., 1998). Variability in $\eta{\cdot}y_S$ corresponds to variability in $E_{i,t=0}$ involved.

When the effectivity η of biomass (production) is maximal, the apparent yield equals the theoretical (maximal) yield y (Eq. (3)). This calculus aligns with authors stating that a 'phenomenological stoichiometry' equals a mechanistic stoichiometry only when the coupling q is maximal (Westerhoff et al., 1982). For the 'same' inoculum, and when other growth substrates are absent, the coupling architecture theoretically accessible for each xenobiotic chemical S is approximately a constant factor (Trapp et al., 2018). Solving for stoichiometry can lead to more than 1 solution for a single S, depending on the prerequisite accuracy of the stoichiometric solution (Eq. (13)). In analogy, differing metabolic routes can lead to similar final products (i.e. CO_2 and H_2O). The routes can differ in effectivity, yield, and in number of metabolic steps. The accuracy of the solution (Eq. (13)), was set at arbitrary values of $\leq 1 \times 10^{-4}$ (Section 3.1.1). The arbitrary criteria however, parallels nature: varying involvement of co-metabolites or co-nutrients may render an exact solution of the stoichiometric impractical: anywhere in the chain metabolism may occur aiding to solve the equation, by

shortcutting the metabolic cycle (Manzoni et al., 2017). This intrinsic feature of our calculus parallels nature: variability can be captured pending more detailed data on cometabolites involved in constituent cycles.

Conventionally, stoichiometric calculation yields rational, fractional integer values for reactants/reagents. This apparently contrasts the results of our calculus (Section 3.1.1), yielding non-integers stoichiometric solutions. The multiple catalytic, signaling and transporting steps by the metabolic machinery will add up along the chain, while transforming only 1 substrate. Likely, machinery is not activated by 1 molecule only, rather, induction needs a certain threshold number (Kovar et al., 2002). Solutions to our simplified stoichiometric calculus may represent only a reduced or minimalized 'projection' of metabolism reflecting primordial or prevolutionary 'life' (Burroughs et al., 2012; Degani and Halman, 1967; Fani, 2012; Laurino et al., 2016; Shitut et al., 2017; Sousa et al., 2013). By a certain probability, bacteria in nature will have available the nutrients (cosubstrates) to apply the shortest or most efficient metabolic path (i.e. solution). Nature parallels our calculus/algorithm, both entailing a probabilistic aspect. Well-fed individuals show a different chemical composition than poorly fed individuals (a function of nutrient consumption) (Brandt, 2002).

5.2. Thermodynamics

We characterized all factors by their elemental compositions. Elements are held together via bonding, the strength of which is quantifiable by bond-dissociation enthalpies ΔH. Phosphorous has a central (phosphatase) signaling role relevant for amino acids, sugars and lipid metabolism (Capra, 2012; Degani and Halman, 1967); protein phosphorylation can (de)activate half of the enzymes present (Vlastaridis et al., 2017). Producing ATP requires investing energy (enthalpy), i.e., phosphorylation by kinases in glycolysis, Figs. 5A–7A. Phosphoanhydride bonds of ATP are stable but upon enzymatic cleavage release energy used to drive cellular machinery (Hunter, 2012; Kamerlin et al., 2013), transport or catalysis, to degrade pollutants. No fundamental limit other than unity can be expected for the thermodynamic efficiency (η=1), but with ATP hydrolysis as driving force a more realistic (maximal) η=0.78 (Astumian, 2019). The majority of our ν values are also $\leq$0.78 (Fig. 5–7; S6).

In a broad sense, entropy is a loss of information. Changes in structural entropy ΔS are a function of the distribution and proportion (apparent surroundings) of each individual atom in the substrate S. The 'octet rule' stipulates that organic substrates can react towards greater complexity than can inorganic substrates. On average, carbon atoms in S (e.g., small alkanes) have less structurally complexity (less rotational/vibrational entropy) than carbon atoms in biomass cofactors $E_{1..x}$ (von Stockar and Liu, 1999). After introduction, microbes can interact to convert $[S]_0$ to biomass cofactors $[E_{1..x}]$, CO_2 (increasing translational entropy), and everything in between (Chaisson, 2011; Mastromatteo et al., 2011). With every transformation, newly produced cofactors E increase overall entropy (arrows in Fig. 2A) (Davies et al., 2013). If resource composition is diverse and abundance constant, evolutionary entropy increases (Demetrius and Gundlach, 2014). Eq. (13) finds an optimal (maximized) quantity for biomass production and, by interpretation, complexity and entropy. The optimization parallels the metabolic chain in Figs. 2A, reaching a maximum.

Certain steps in metabolic chains are repeated (iterated): after metabolizing the parent substrate S_0, its metabolite S' may require a different enzyme for catalysis and will therefore (again) diffuse or be transported, e.g. in and out a specialized cell (compartment) or enzyme, binding to different (oxygenase) active sites (Eq. (2)) (McCarty, 2007). Since S_0 and S' have similar structures (by definition), Gibbs free energy changes ΔG for transformation ($S_0 \rightarrow S'$) are likely to be proportional to subsequent transformations (S' $\rightarrow$ S'', etc.). A bacterium likely first metabolizes S via the highest (Gibbs) energy gain, and subsequently metabolizes the formed metabolite via its highest energy gain, etc. In

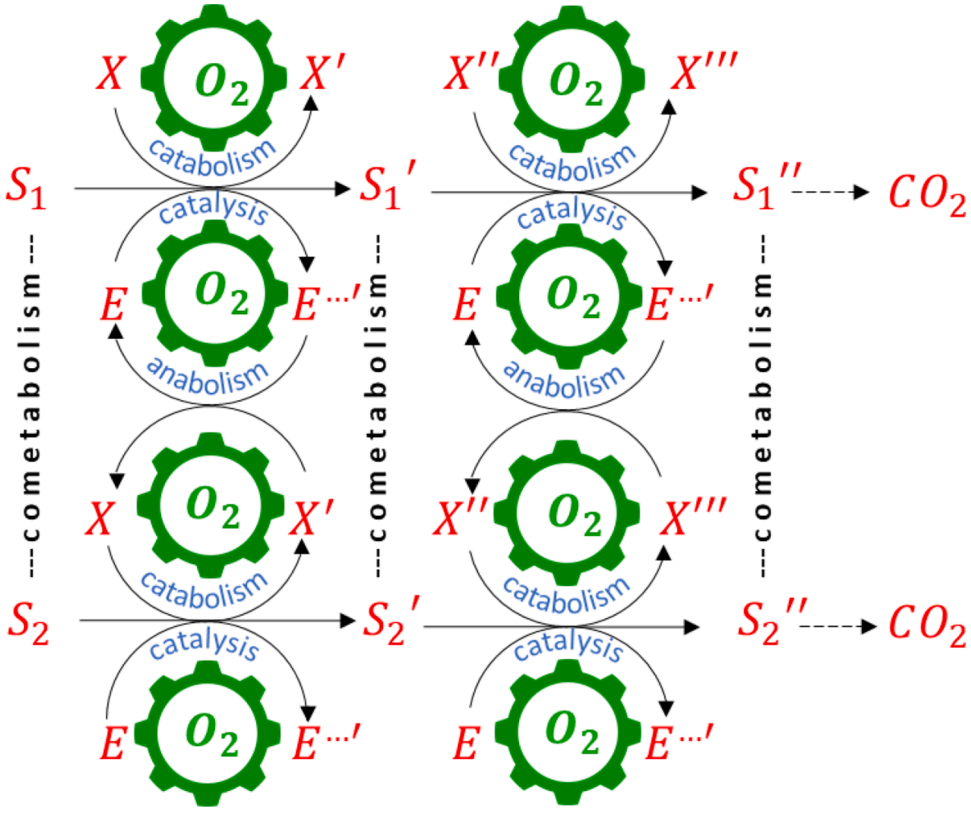

Fig. 9. Schematic visualization of metabolic machinery involved in pollutant (substrate S) biodegradation. The sizes of the arrows are indicative of the stoichiometry. The presence and abundance of suitable E and X (cogs) represent acclimation.

this way, any change in partial Gibbs energy ΔG is a portion of the previous one (substantiating Figs. 1, 2). As such, $\eta \cdot y$ would decrease exponentially with the number of steps that preceded the metabolite, i.e., 'biodegradation coordinate' (Figs. 1, 2). Further along this coordinate, resistance decreases as the substrate becomes increasingly 'natural'. With exceptions, natural metabolites tend to have lower energies than nonbiological molecules (Jinich et al., 2020).

Gibbs energy losses entail entropic loss, water/solvent reorganization, inert side products, synthesizing/maintaining enzymes, co-factors/nutrients. Converting S to E becomes less efficient when the number of steps from S to E_i increases. The amount of 'work' needed thus depends on how much the microbial consortia has acclimated (it's E) to degrade S. Then, degradation (time) depends on the manner by which the system changes from one state to another. Thermodynamically, acclimation would be a 'path function' or 'process function', Fig. 2: the route by which a system goes from state A to state B determines the result. ηy_s is proportional to some resistance along a path of metabolic steps, wherein cofactors are needed to embed the substrate into the endemic metabolism. Usually, peripheral metabolic reactions (oxygenases) are less efficient than are central metabolic reactions, where energy is produced for cell functioning (González-Cabaleiro et al., 2015).

5.3. Metabolism

Bacteria compete for substrates, which can only 'feed' bacteria if their concentration is 'high enough' so to induce a metabolic response. That is, relative to (and 'competing' with) other biodegradable (carbonaceous) chemicals (e.g. small carbohydrates) (Quiroga, 1994; Nolte et al., 2018), Eq. (4–6). The strength of the correlations, decreasing in the order of carbohydrates > nucleotides > lipids > amino acids (Figs. 5;6), may correspond to natural concentrations. Carbohydrates make up the bulk of biomass: around 90% of the dry weight of gram-positive bacteria is peptidoglycan (10% for gram-negative); and peptidoglycan consists ~50% of sugar. The polysaccharide glycogen is also a short-term energy storage (Berg et al. 2002). Aldose sugars have the highest possible number of redox connections to other molecules (Jinich et al., 2020). Glycolysis of glucose gives pyruvate; with oxaloacetate partake in the citric acid cycle, gluconeogenesis, the urea cycle, the glyoxylate cycle, amino acid synthesis and fatty acid synthesis. Combined, this may explain high correlations for carbohydrates (Figs. 5, Fig. 6) (Elsemman et al., 2021). Similarly, apparent correlation for carboxylates (Fig. 6) denotes decarboxylation (electron transfer) as a distinct (final) step of a metabolic path (González-Cabaleiro et al., 2015; Huwiler et al., 2019; Saylor et al., 2012).

Nutrient deficiency may prompt microorganisms to use other energy stores, such as polyhydroxyalkanoates (Kim and Lenz, 2001). Instead of transformation, bacteria may accumulate (embed) or store fatty acids (lipids) in membranes or micelles (Dodds, 1991). This involves weak (van de Waals) bonds (Arantes et al., 2020), rather than breaking/forming covalent bonds (parabola intersections in Fig. 2). Rather than active respiratory processes, lipids represent (long-term) 'reserves', e.g. as in DEB metabolic models. Then, lipid metabolism comes into play when the endemic bacterial consortium is under pressure (Garton et al., 2008). This may help to explain the negative sign of the correlations for lipids (Figs. 5,Fig. 6). If only catabolism were involved, we would not see a concentration dependance; therefore v must represent (also) anabolism and/or cometabolism (Dalton and Stirling, 1982; Luo et al., 2014). Coupling between metabolic chains distinguishes catabolism from anabolism (Shitut et al., 2017; Westerhoff et al., 1982), Fig. 9. Indeed, co-metabolism enhances k significantly (Fig. S6), Fig. 9. The versatile coenzyme A serves both anabolic and catabolic functions, prominently involving fatty acids.

A xenobiotic structurally similar to a natural substrate binds to $E_{1\ldots x}$ (receptors, enzymes, etc.) but may not be (immediately) transformed. Still, it may induce (up- or down regulate) more $E_{1\ldots x}$ (e.g., transporters) that, indirectly (in the end) do facilitate transformation (Kim, 2002; Klaassen and Lu, 2008; Narang et al., 2008). A plethora of transport systems exist, some of which induced by individuals in the population through bet hedging. Microorganisms may scavenge any suitable scarce substrate, as long as it enables them to outcompete competitors. The microbial world is also rich in catalytic capabilities: able to catabolize (m)any compound(s) to harvest energy if at all possible (Hadadi et al., 2019). Higher biodiversity maximizes the collective potential for biotransformation, prominently for rare pollutants (Jaeger et al., 2019; Johnson et al., 2015). Some transporters and enzymes (locks and keys) are less than fully specific (about half of reactions lack an associated protein sequence or gene) (Hadadi et al., 2019), allowing other than their cognate substrates to pass or even be accumulated. Some chemical activation systems enable priming of hard to degrade compounds such as through mixed function oxidation.

5.4. Cofactors x

Correlations were relatively strong for nucleic acids (Figs. 5,6), representing transformation of S to biomass E via cofactors X. No compound is biodegradable by itself; microbes often need cofactors (X) for enzymes to function, Fig. 9. Substrates S and cofactors X complement each other. N-rich substrates (e.g., nucleotide analogs) need C-rich cofactors (i.e., carbohydrates), and vice versa: N-rich cofactors 'needed' determines the proportion of C-rich S_0 that is incorporable (via S', S'', etc.) as E, Eq. (2). Most cofactors frequently involved in metabolic reactions (e.g., dehydrogenases) contain nitrogen, (flavins/hemes NADP, FAD(H), FMN, coenzyme A and ATP, kinases) (Huwiler et al., 2019) as a bio-active element (Pennington and Moustakas, 2017) affecting biodegradation (Nolte et al., 2018). Metabolism continuously makes and breaks nitrogen-carbon (e.g., glycosidic) bonds involving many 'general' enzymes (e.g. NAD synthesis from tryptophan/aspartate). Adenosine cofactors catalyze many (redox) reactions like methyl, acyl, and phosphoryl group transfer.

ATP is produced by catabolism and consumed by anabolism (Westerhoff et al., 1982); its measurement helps quantifying presence and abundance active/viable biomass (e.g., for water treatment) (Apoteker and Thevenot, 1983; Knezev and van der Kooij, 2004; Kyriakides et al., 1991; Nguyen et al., 2018; Stoddart et al., 2016). Oxidative phosphorylation produces ATP by shuffling NAD(H) and FAD(H) used in the electron transport chain (i.e., coenzyme Q_{10}). Many cofactors entail (di) nucleotides (NAD(H), FAD(H)), produced by the citric acid cycle; oxidation of NADH and succinate ($C_4H_6O_4$); powers ATP synthase. The signaling molecule succinate links cellular metabolism, esp. ATP production, to cellular function (regulation). Transformation ($S_0 \rightarrow S'$) of sugars (i.e. glycolysis), amino acids and vitamins ($v_{S\mathrm{CH}} = 0.7–0.8$) normally involves only 1 or 2 ATP molecules (Teusink et al., 2006), but full mineralization (sugar to CO_2) i.e., respiration involves ~36 ATP. In these respects, our calculus is a measure of the viability of a cell's investment of using S to generate growth via S', S'', etc. (Cornelissen and Sijm, 1996; Lijklema, 1971).

Stoichiometry v_s affects acclimation (i.e., biodegradation) by orders of magnitudes (Figs. 5–7). Although the variation in v_s is only ~0.5 (Figs. 5–7), stoichiometric mismatch can add up along potentially billions of metabolic reactions, 0.5^9, to affect rates by three orders of magnitude ($0.5^9 \approx 10^{-3}$) (Adadi et al., 2012). It is not uncommon to see slight modifications lead to 100-fold change in functions and rates (Griffiths, 2003; Sreedhara et al., 2000; Walkiewicz et al., 2012). Changing only a few residues (i.e. small changes in v_s) in a substrate can greatly decrease catalytic efficiency, and hence halt the metabolic chain (Newton, 2015). Nature can then tap into a larger sequence space, to create catalytic activity (Davies et al., 2013; Renata et al., 2015). Results of our calculus (the exponent of 9) may represent feedback mechanisms (loops) among the metabolic steps (Schwahn et al., 2017), indirectly involving billions of potential (0.5^9) cofactors X and E. In comparison, cells contain ~$0.1–1 \times 10^7$ proteins (Ho et al., 2018; Milo, 2013), $>3 \times 10^5$ distinct CYP proteins are known (Nelson, 2018), many of these

require cofactors X (binding to the universal Rossmann fold) (Laurino et al., 2016). Strictly, a catalyst is all that speeds up reaction but is not consumed or can be easily regenerated. In this sense, what functionally and physically distinguishes biomass cofactors E from X may sometimes seem arbitrary (metallic ions, (co)enzymes, prosthetic groups, etc.).

5.5. Outlook

'Naturalness' is defined as "produced or existing in nature", in contrast to 'artificial' (All natural 2007). As natural subunits can be combined into an anthropogenic chemical, the distinction is not categorial, but continuous (color changes in Table 2; Fig. 2). From an evolutionary perspective, 'unnatural' xenobiotics were recently introduced to the environment and have no dedicated transporters or metabolic pathways. Acclimation then occurs over years of selection pressure: beneficial mutations in order to use a substrate are accumulated while aggrupation of genes inside the same degradation pathway (Hadadi et al., 2019; Knott et al., 2020). Study on naphthalene hydrocarbons ([S]>1 mg/L) gave $\eta{\cdot}y_S \approx 0.4$ (Knightes and Peters, 2000) (contrasting our v_s) implying that our scope (<1 mg/L) still needs widening in future (Trapp et al., 2018), e.g. via bioconcentration (Fig. 8). Toxic substrates are not 'natural', as S could not have been present while the microbe developed. S may interfere with metabolism to result in cell death if not detoxified (e.g., degraded). Antimicrobials and organophosphates exert growth inhibition at concentrations lower than 1 mg/L. Haldane kinetics describes such inhibition (Gaszczak et al., 2012; Perales et al., 1999) constituting the basis of Eq. (4). Thereby, future study may incorporate (mixture) toxicity via the toxic unit approach (De Zwart, 2002; Nolte et al., 2020b) to further detail the active biomass.

Concentrations vary in situ due to diffusion (e.g. floc size), redox/oxygen and temperature, needing consideration (Brandt and Kooijman, 2000; Chen et al., 2017; Perales et al., 1999a), e.g. via allometric scaling (Mulder and Hendriks, 2014). Glucose as a benchmark, we can interpolate results to anaerobic conditions: fermentation to lactate (2 ATP) produces ~20 times less ATP than does oxidation to CO_2 (~36). Measuring concentration enables selecting appropriate kinetic laws (Hardin et al., 2009). Rather than $i = 1$–5, a more complete solution to Eq. (15), requires knowing concentrations of metabolic cofactors E involved, to extend the summation operator (Eq. (10)) (Bennett et al., 2008). Sulfur metabolism (e.g. furosemide in Fig. 7) may require separate parametrization (Eq. 17), e.g. pH hydrolysis (Knott et al., 2020; Yagi et al., 1991). Concentrations do not *a priori* extrapolate to metabolic involvement, activity or turnover: DEB theory could aid, providing rules for energy fluxes, exploiting conservation laws and stoichiometric constraints accounting for reserves and maintenance (Brandt, 2002). We might then incorporate metabolic mapping to weigh the numerators in Eq. (15) based on flux balances (Elsemman et al., 2021; Lee et al., 2006; Nielsen, 2003). As bacteria have genetic, anatomical and functional similarity to mitochondria (endosymbiosis) (Pallen, 2011), we may use in vitro (hepatic) transformation data (k_{cat}/K_s) to corroborate, broaden and refine our calculus by calibrating specific metabolic machinery.

Algebraic solutions have finite applicability. Without experimentally testing the dimensions of applicability, we cannot know the truth. Cells detect, transport and -form compounds via complex signaling machinery and pathways. Bacteria synthesize compounds by organized metabolic networks with intricately coupled catalytic and transport systems. Conversely, biodegradation is notoriously complex, cumbersome to characterize, monitor and understand in detail (via omics). We cannot realistically characterization and monitor all (variable (sub)structures of) cometabolites and cofactors, but quantifying them in terms of elemental composition (e.g., atomic spectroscopy), is straightforward. Experimentation is not ideal for (large) volume predictions and screening (Bennett et al., 2008). Our approach/calculus actively identifies properties promoting biodegradation, thereby helping screening, prioritizing and sorting 'green' chemicals among 10.000+ industrial 'grey' chemicals (Rucker and Kummerer, 2012; Sharma et al., 2008) (Figs. 2–4). Results of the current study illustrate a useful computationally inexpensive tool to design, select and monitoring (real-life) substances aiding green chemistry and implement its principles (Rucker and Kummerer, 2012).

6. Conclusion

In this study we opted to refine by redefining biodegradation models. We developed calculus and algebra for experimentally derived effective η yield y_S of biomass cofactors E production from a compound substrate S: $\eta{\cdot}y_S$. It captures acclimation state and influence of S concentration on a kinetic rate constant k (Eq. 1). We also calculated stoichiometric ratios v_S, as a 'likeness', (e.g., scoring similarity of S to biomass E) 'naturalness', (Fig. SI) or inverse 'resistance' along metabolic chains (Fig. 3, Table 2): if the xenobiotic does not 'resemble' biomass cofactor E, more co-substrates X are needed. A relationship exists between $\eta{\cdot}y_S$ and v_S. Predictions based thereon are biologically and chemically intuitive, requiring (e.g., experimental monitoring) input in the form of elemental concentrations of potential cofactors. Increasing the concentration of an E stoichiometrically similar to S, or adding co-substrates X, decreases the half-life of S. The stronger correlation for EpiSuite data (Fig. 5) as compared to other (in-house) data (Fig. 6;7) may be due to EpiSuite data containing more information on complete metabolism, i.e., mineralization to CO_2 and H_2O (more resistance along, and coupling between more steps 1…x). It may also entail more information on nitrogen metabolism (vs. carbohydrate) as N concentrations in wastewater are usually higher (Carey and Migliaccio, 2009), and may also reflect anaerobic-anaerobic differences (van Lier et al., 2008).

We evaluated predictions of $\eta{\cdot}y_S$ via v_S in real-life scenarios for biodegradation in wastewater and surface water. The maximum correlation (prediction precision) that can be expected based on uncertainty in experimental $\eta{\cdot}y_S$ is 30–40%. In comparison, we found a maximal 20–30% correlation with predicted v_s (Figs. 5–7). In other words, 20–30% of the variation in $\eta{\cdot}y_S$ can be accounted for by v_S (in terms of R^2). Parallels between theory, algebra and observed phenomena (Sections 5.1–5.4), indicate that our new approach has good accuracy, (extrapolative) power, and is capable of generating predictions. Combined, it predicts degradation more accurately than existing empirical relations, prominently for substances outside the domain of those empirical relations. Existing biodegradation models often treat co-metabolism by adding (empirical) substrate (and experiment-) specific parameters to fit the observed kinetics (Brandt, 2002). Case studies apply stoichiometric constraints for a limited set of substrates (S) and conditions (~E) (Lobo et al., 2013). Examples illustrate that stoichiometry drives metabolism across different scientific subdisciplines (Filipiak et al., 2017). Our generalization helps to establish a mechanistic basis of understanding, minimizing the need for (empirical) fitting. Co-metabolism is intrinsically embedded in our approach, as 'naturalness' reflects the presence of metabolic cofactors E (enzymes, transporters, etc.). Biodegradation in a different setting involves adapting the set of cofactors E_i and re-running the algebra. Environmental fate assessment frameworks often assume steady-state conditions (European Community, 2003; EPA, 2008), which applies also to our method too. Its results demonstrate implementation to screen, assess and optimize 'green' chemicals.

Declaration of Competing Interest

The authors declare that they have no conflicts of interest.

Acknowledgements

This work is part of the research program TTW financing the Contaminants of Emerging Concern in the Water Cycle (CERCEC) project number 15759, which is financed by the Dutch Research Council (NWO).

Supplementary materials

Supplementary material associated with this article can be found, in the online version, at doi:10.1016/j.watres.2022.118333.

References

Achermann, S., Mansfeldt, C.B., Müller, M., Johnson, D.R., Fenner, K., 2020. Relating metatranscriptomic profiles to the micropollutant biotransformation potential of complex microbial communities. Environ. Sci. Technol. 54 (1), 235–244.

Adadi, R., Volkmer, B., Milo, R., Heinemann, M., Shlomi, T., 2012. Prediction of microbial growth rate versus biomass yield by a metabolic network with kinetic parameters. PLoS Comput. Biol. 8 (7), e1002575.

Ahtiainen, J., Aalto, M., Pessala, P., 2003. Biodegradation of chemicals in a standardized test and in environmental conditions. Chemosphere 51 (6), 529–537.

Alves, L.F., et al., 2018. Metagenomic approaches for understanding new concepts in microbial science. Int. J. Genom. 2018, 2312987.

All natural, 2007. Nat. Chem. Biol. 3 (7), 351. https://doi.org/10.1038/nchembio0707-351.

Apoteker, A., Thevenot, D.R., 1983. Experimental simulation of biodegradation in rivers. Water Res. 17 (10), 1267–1274.

Arantes, P.R., Polêto, M.D., Pol-Fachin, L., Verli, H., 2020. The lazy life of lipid-linked oligosaccharides in all life domains. J. Chem. Inf. Model. 60 (2), 631–643.

Astumian, R.D., 2019. Kinetic asymmetry allows macromolecularcatalysts to drive an information ratchet. Nat. Commun. 10.

Balcom, I.N., Driscoll, H., Vincent, J., Leduc, M., 2016. Metagenomic analysis of an ecological wastewater treatment plant's microbial communities and their potential to metabolize pharmaceuticals. F1000Res 5, 1881.

Bar-Even, A., et al., 2011. The moderately efficient enzyme: evolutionary and physicochemical trends shaping enzyme parameters. Biochemistry 50 (21), 4402–4410.

Berg, J.M., Tymoczko, J.L., Stryer, L., 2002. Chapter 21 - Glycogen Metabolism. In: Biochemistry, 5th Edition. WH Freeman, New York.

Bennett, B.D., Yuan, J., Kimball, E.H., Rabinowitz, J.D., 2008. Absolute quantitation of intracellular metabolite concentrations by an isotope ratio-based approach. Nat. Protoc. 3 (8), 1299–1311.

Boethling, R.S., et al., 1994. Group-contribution method for predicting probability and rate of aerobic biodegradation. Environ. Sci. Technol. 28 (3), 459–465.

Brandt, B.W., 2002. Realistic Characterizations of Biodegradation. PhD Thesis. Vrije Universiteit Amsterdam.

Brandt, B.W., Kooijman, S.A.L.M., 2000. Two parameters account for the flocculated growth of microbes in biodegradation assays. Biotechnol. Bioeng. 70 (6), 677–684.

Burroughs, L., et al., 2012. Asymmetric organocatalytic formation of protected and unprotected tetroses under potentially prebiotic conditions. Org. Biomol. Chem. 10 (8), 1565–1570.

Canela, E.I., Navarro, G., Beltrán, J.L., Franco, R. 2019. The meaning of the Michaelis-Menten constant: Km describes a steady-state. bioRxiv. https://doi.org/10.1101/608232.

Capra, E.J.and Laub.M.T., 2012. Evolution of two-component signal transduction systems. Annu. Rev. Microbiol. 66, 325–347.

Carey, R.O., Migliaccio, K.W., 2009. Contribution of wastewater treatment plant effluentsto nutrient dynamics in aquatic systems: a review. Environ. Manage. 44, 205–217.

Chai, J.H., et al., 2018. Cost-benefit analysis of introducing next-generation sequencing (metagenomic) pathogen testing in the setting of pyrexia of unknown origin. PLoS One 13 (4), e0194648.

Chaisson, E.J., 2011. Energy rate density as a complexity metricand evolutionary driver. Complexity 16 (3), 27–40.

Chen, J.W., et al., 2017. Impacts of chemical gradients on microbial community structure. ISME J. 11 (4), 920–931.

Chong, N.M., Tsai, S.C., Le, T.N., 2010. The biomass yielding process of xenobiotic degradation. Bioresour. Technol. 101 (12), 4337–4342.

Chong, N.M., Wang, C.H., Ho, C.H., Hwu, C.S., 2011. Xenobiotic substrate reduces yield of activated sludge in a continuous flow system. Bioresour. Technol. 102 (5), 4069–4075.

Cornelissen, G., Sijm, D.T., 1996. An energy budget model for the biodegradation and cometabolism of organic substances. Chemosphere 33 (5), 817–830.

Dalton, H., Stirling, D.I., 1982. Co-metabolism. Philos. Trans. R. Soc. Lond. Series B 297 (1088), 481–496.

Davies, P.C., Rieper, E., Tuszynski, J.A., 2013. Self-organization and entropy reduction in a living cell. Biosystems 111 (1), 1–10.

De Zwart, D., 2002. Observerd regularities in SSDs for aquatic species. Species sensitivty distributions in ecotoxicology. In: Posthuma, L., Suter, G., Traas, T. (Eds.), Species Sensitivty Distributions in Ecotoxicology. Lewis Publisher, Boca Raton, FL, USA, pp. 133–154.

De Zwart, D., Posthuma, L., 2005. Complex mixture toxicity for single and multiple species: proposed methodologies. Environ. Toxicol. Chem. 24 (10), 2665–2676.

Degani, C.H., Halman, M., 1967. Chemical evolution of carbohydrate metabolism. Nature 216 (5121), 1207.

Demetrius, L.A., Gundlach, V.M., 2014. Directionality theory and the entropic principle of natural selection. Entropy 16, 5428–5522.

Directive 2000/60/EC of the European Parliament and of the Council of 23 October 2000 establishing a framework for Community action in the field of water policy Official Journal L 327, 22/12/ 2000 0001 - 0073.

Dodds, P.F., 1991. Incorporation of xenobiotic carboxylic acids into lipids. Life Sci. 49 (9), 629–649.

ECHA: European Chemicals Agency, 2020. Annual Report 2019. ECHA-20-R-04-EN. ISBN: 978-92-9481-399-2.

Elsemman, I.E. et al., 2021. Whole-cell modeling in yeast predicts compartment-specific proteome constraints that drive metabolic strategies. bioRxiv(Corpus ID: 235418823).

EPA, 2008. OPPTS 835.3280 Simulation Tests to Assess the Primary and Ultimate Biodegradability of Chemicals Discharged to Wastewater. 712-C-08-00.

European Community, 2003. Technical Guidance Document on Risk Assessment in support of Commission Directive 93/67/EEC on Risk Assessment for new notified substances Commission Regulation (EC) No 1488/94 on Risk Assessment for existing substances.

Evenblij, H., Schuman, E., Kuiper, M., 2020. Verwijderingsrendementen van medicijnresten op 18 rwzi's. WDOD database. Water Matters 28–31.

Eyring, H., 1935. The Activated Complex in Chemical Reactions. J. Chem. Phys. 3 (2), 107–115.

Fagerbakke, K.M., Heldal, M., Norland, S., 1996. Content of carbon, nitrogen, oxygen, sulfur and phosphorus in native aquatic and cultured bacteria. Aquat. Microb. Ecol. 10 (1), 15–27.

Fani, R., 2012. The origin and evolution of metabolic pathways: why and how did primordial cells construct metabolic routes? Evolution 5, 367–381.

Ferraz de Arruda, G., Cozzo, E., Rodrigues, F.A., Moreno, Y., 2018. A polynomial eigenvalue approach for multiplex networks. New J. Phys. 20, 095004.

Filipiak, M., et al., 2017. Ecological stoichiometry of the honeybee: pollen diversity and adequate species composition are needed to mitigate limitations imposed on the growth and development of bees by pollen quality. PLoS One 12 (8), e0183236.

Garton, N.J.W.S.J., Sherratt, A.L., Lee, S., Smith, R.J., Senner, C., Hinds, J., Rajakumar, K., Adegbola, R.A., Besra, G.S., Butcher, P.D., Barer, M.R., 2008. Cytological and transcript analyses reveal fat and lazy persister-like bacilli in tuberculous sputum. PLoS Med. 5 (4), e75.

Gaszczak, A., Bartelmus, G., Gren, I., 2012. Kinetics of styrene biodegradation by Pseudomonas sp E-93486. Applied Microbiology and Biotechnology 93 (2), 565–573.

González-Cabaleiro, R., Ofiţeru, I.D., Lema, J.M., Rodríguezm, J., 2015. Microbial catabolic activities are naturally selected by metabolic energy harvest rate. ISME J. 9, 2630–2641.

Griffiths, A.D.andTawfik .D.S., 2003. Directed evolution of an extremely fast phosphotriesterase by in vitro compartmentalization. EMBO J. 22 (1), 24–35.

Hadadi, N., MohammadiPeyhani, H., Miskovic, L., Seijo, M., Hatzimanikatis, V., 2019. Enzyme annotation for orphan and novel reactions using knowledge of substrate reactive sites. Proc. Natl. Acad. Sci. U S A, 116 (15), 7298–7307.

Haldane, J.B.S., 1930. Enzymes. Longmans, Green, London.

Hardin, H.M., Zagaris A., Krab, K., Westerhoff, H.V., 2009. Simplified yet highly accurate enzyme kinetics for cases of low substrate concentrations. FEBS J. 276, 5491–5506.

Hendriks, A.J., 2016. Chapter 7: Organisms. Syllabus for Environmental and Ecological Modelling, p. 79.

Hill, T.L., 1976. Diffusion frequency factors in some simple examples of transition-state rate theory. Proc. Natl. Acad. Sci. U.S.A. 73 (3), 679–683.

Ho, B., Baryshnikova, A., Brown, G.W., 2018. Unification of protein abundance datasets yields a quantitative saccharomyces cerevisiae proteome. Cell Syst. 6, 192–205.

Hunter, T., 2012. Why nature chose phosphate to modify proteins. Philos. Trans. Royal Soc. B 367 (1602), 2513–2516.

Huwiler, S.G., et al., 2019. One-megadalton metalloenzyme complex in Geobacter metallireducens involved in benzene ring reduction beyond the biological redox window. Proc. Natl. Acad. Sci. U S A, 116 (6), 2259–2264.

Jaladanki, C.K., et al., 2020. Mechanistic studies on the drug metabolism and toxicity originating from cytochromes P450. Drug Metab. Rev. 52 (3), 366–394.

Jaeger, A., et al., 2019. Using recirculating flumes and a response surface model to investigate the role of hyporheic exchange and bacterial diversity on micropollutant half-lives. Environ. Sci. (21), 2093.

Jinich, A., et al., 2018. Quantum chemistry reveals thermodynamic principles of redox biochemistry. PLoS Comput. Biol. 14 (10), e1006471.

Jinich, A., et al., 2020. A thermodynamic atlas of carbon redox chemical space. Proc. Natl. Acad. Sci. U. S. A. 117 (52), 32910–32918.

Johnson, D.R., et al., 2015. Association of biodiversity with the rates of micropollutant biotransformations among full-scale wastewater treatment plant communities. Appl. Environ. Microbiol. 81 (2), 666–675.

Kamerlin, S.C.L., Sharma, P.K., Prasad, R.B., Warshel, A., 2013. Why nature really chose phosphate. Q. Rev. Biophys. 46 (1), 1–132.

Karki, S.B., Dinnocenzo, J.P., 1995. On the mechanism of amine oxidations by P450. Xenobiotica 25 (7), 711–724.

Kim, R.B., 2002. Transporters and xenobiotic disposition. Toxicology 182-182, 291–297.

Kim, Y.B., Lenz, R.W., 2001. Polyesters from microorganisms. Adv. Biochem. Eng. Biotechnol. 71, 51–79.

Klaassen, C.D., Lu, H., 2008. Xenobiotic transporters: ascribing function from gene knockoutand mutation studies. Toxicol. Sci. 101 (2), 186–196.

Knezev, A., van der Kooij, D., 2004. Optimisation and significance of ATP analysis for measuring active biomass in granular activated carbon filters used in water treatment. Water Res. 38 (18), 3971–3979.

Knightes, C.D., Peters, C.A., 2000. Statistical analysis of nonlinear parameter estimation for Monod biodegradation kinetics using bivariate data. Biotechnol. Bioeng. 69 (2), 160–170.

Knott, B.C., et al., 2020. Characterization and engineering of a two-enzyme system for plastics depolymerization. Proc. Natl. Acad. Sci. U S A, 117 (41), 25476–25485.

Kovar, K., Chaloupka, V., Egli, T., 2002. A Threshold Substrate Concentration Is Required to Initiate the Degradation of 3-Phenylpropionic Acid in Escherichia coli. Acta Biotechnol. 22 (3–4), 285–298.
Kowalczyk, A., et al., 2015. Refinement of biodegradation tests methodologies and the proposed utility of new microbial ecology techniques. Ecotoxicol. Environ. Saf. 111, 9–22.
Kumar, A., Sharma, S.K., Sharma, G., Naushad, M., Stadler, F.J., 2020. CeO2/g-C3N4/V2O5 ternary nano hetero-structures decorated with CQDs for enhanced photo-reduction capabilities under different light sources: dual Z-scheme mechanism. J. Alloys Compd. 838, 155692.
Kyriakides, A.L., Costello S.M.,, Doyle G, Easter, M.C., Johnson, I., 1991. Rapid hygiene monitoring using ATP bioluminescence. In: PE, S., LJ, K. (Eds.), Bioluminescence and Chemiluminescence: Current Status. Wiley Chichester, pp. 519–522.
Laurino, P., et al., 2016. An ancient fingerprint indicates the common ancestry of rossmann-fold enzymes utilizing different ribose-based cofactors. PLoS Biol. 14 (3), e1002396.
Leder, C., Rastogi, T., Kummerer, K., 2015. Putting benign by design into practice-novel concepts for green and sustainable pharmacy: designing green drug derivatives by non-targeted synthesis and screening for biodegradability. Sustain. Chem. Pharm. 2, 31–36.
Lee, J.M., Gianchandani, E.P., Papin, J.A., 2006. Flux balance analysis in the era of metabolomics. Brief Bioinform. 7 (2), 140–150.
Li, Z., McLachlan, M.S., 2019. Biodegradation of Chemicals in Unspiked Surface Waters Downstream of Wastewater Treatment Plants. Environ. Sci. Technol. 53 (4), 1884–1892.
Lijklema, L., 1971. Factors affecting pH change in alkaline wastewater treatment - II. Carbon dioxide production. Water Res. 5, 123–142.
Lim, B.R., Huang, X., Hu, H.Y., Goto, N., Fujie, K., 2001. Effects of temperature on biodegradation characteristics of organic pollutants and microbial community in a solid phase aerobic bioreactor treating high strength organic wastewater. Water Sci. Technol. 43 (1), 131–137.
Lobo, C.C., Bertola, N.C., Contreras, E.M., 2013. Stoichiometry and kinetic of the aerobic oxidation of phenolic compounds by activated sludge. Bioresour. Technol. 136, 58–65.
Lunghini, F., et al., 2020. Modelling of ready biodegradability based on combined public and industrial data sources. SAR QSAR Environ. Res. 31 (3), 171–186.
Luo, L., Meng H.,, Gu, J., 2017. Microbial extracellular enzymes in biogeochemical cycling of ecosystems. Environ. Manage. 197, 539–549.
Luo, W., et al., 2014. Mechanisms and strategies of microbial cometabolism in the degradation of organic compounds - chlorinated ethylenes as the model. Water Sci. Technol. 69 (10), 1971–1983.
Ma, D., et al., 2021. Critical review of advanced oxidation processes in organic wastewater treatment. Chemosphere 275, 130104.
Maggi, F., la Cecilia, D., 2016. Implicit analytic solution of Michaelis-Menten-Monod kinetics. ACS Omega 1 (5), 894–898.
Manzoni, S., et al., 2017. Optimal metabolic regulation along resource stoichiometry gradients. Ecol. Lett. 20, 1182–1191.
Mastromatteo, U., Pasquinelli, P., Giorgetti, A., 2011. Thermodynamics, information, and complexity in artificial and living systems. WIT Trans. State Art Sci. Eng. 51, 119.
McCarty, P.L., 2007. Thermodynamic electron equivalents model for bacterial yield prediction: modifications and comparative evaluations. Biotechnol. Bioeng. 97 (2), 377–388.
Mendes-Felipe, C., Veloso-Fernández, A., Vilas-Vilela, J.L., Ruiz-Rubio, L., 2022. Hybrid Organic–Inorganic Membranes for Photocatalytic Water Remediation Catalysts, 12 (2): 180.
Mishra, B., et al., 2020. Omics approaches to pesticide biodegradation. Energy Environ. 0 (0), 1–30.
Milo, R., 2013. What is the total number of protein molecules per cell volume? A call to rethink some published values. Bioessays 35 (12), 1050–1055.
Monod, J., 1942. Recherches Sur La Croissance Des Cultures Bactériennes. Hermann, Paris.
Mulder, C., Hendriks, A.J., 2014. Half-saturation constants in functional responses. Glob. Ecol. Conserv. 2, 161–169.
Narang, V.S., et al., 2008. Dexamethasone increases expression and activity of multidrug resistance transporters at the rat blood-brain barrier. Am. J. Physiol. Cell Physiol. 295 (2), 440–450.
Nazzal, G., 2016. The relative values of the turnover number and the dissociation rate constant determine the definition of the Michaelis-constant. bioRxiv. doi:10.1101/052514.
Nelson, D.R., 2018. Cytochrome P450 diversity in the tree of life. Biochim. Biophys. Acta Proteins Proteom. 1866 (1), 141–154.
Newton, M.S.A.V.L., Patrick, W.M., 2015. Rapid bursts and slow declines: on the possible evolutionary trajectories of enzymes. J. R. Soc.. Interface 12 (107), 20150036.
Nguyen, H.L., Chong, M.N., Bui, H.M., 2018. Shortening the acclimation and degradation lag of xenobiotics by enriching the energy content of microbial populations. Pol. J. Environ. Stud. 27 (6), 2893–2897.
Nielsen, J., 2003. It is all about metabolic fluxes. J. Bacteriol. 185 (24), 7031–7035.
Nolte, T.M., et al., 2020a. Disentanglement of the chemical, physical, and biological processes aids the development of quantitative structure-biodegradation relationships for aerobic wastewater treatment. Sci. Total Environ. 708.
Nolte, T.M., Chen, G., et al., 2020a. Disentanglement of the chemical, physical, and biological processes aids the development of quantitative structure-biodegradation relationships for aerobic wastewater treatment. STOTEN 708, 133863.
Nolte, T.M., Nauser, T., Gubler, L., Peijnenburg, W.J.G.M., et al., 2020ba. Thermochemical unification of molecular descriptors to predict radical hydrogen abstraction with low computational cost. PCCP 22 (40), 23215–23225.
Nolte, T.M., Novak, L.,, Hendriks, A.J., Peijnenburg, W.J.G.M., 2021. A universal free energy relationship for both hard and soft radical addition in water. J. Phys. Chem. A 35 (4), 2022e431.
Nolte, T.M., Nauser, T., Gubler, L., Peijnenburg, W.J.G.M., 2020bb. Thermochemical unification of molecular descriptors to predict radical hydrogen abstraction with low computational cost. PCCP 22 (40), 23215–23225.
Nolte, T.M., Peijnenburg, W.J.G.M., Bergen, T.J.H.M.v., Hendriks, A.J., 2020c. Transition-state rate theory sheds light on 'black-box' biodegradation algorithms. Green Chem.
Nolte, T.M., Pinto-Gil, K., Hendriks, A.J., Ragas, A.M.J., Pastor, M., 2018. Quantitative structure-activity relationships for primary aerobic biodegradation of organic chemicals in pristine surface waters: starting points for predicting biodegradation under acclimatization. Environ. Sci. 20 (1), 157–170.
Nolte, T.M., Ragas, A.M.J., 2017. A review of quantitative structure-property relationships for the fate of ionizable organic chemicals in water matrices and identification of knowledge gaps. Environ. Sci. 19 (3), 221–246.
Nyholm, N., 1991. The European system of standardized legal tests for assessing the biodegradability of chemicals. Environ. Toxicol. Chem. 10 (10), 1237–1246.
Ouiroga, J.M., Perales .J.A., Romero, L.I., Sales, D., 1999. Biodegradation kinetics of surfactants in seawater. Chemosphere 39 (11), 1957–1969.
Pagga, U., 1997. Testing biodegradability with standardized methods. Chemosphere 35 (12), 2953–2972.
Pallen, M.J., 2011. Time to recognise that mitochondria are bacteria? Trends Microbiol. 19, 58–64.
Paniagua-Michel, J., Olmos-Soto, J., 2016. Modern Approaches into Biochemical and Molecular Biomarkers: key Roles in Environmental Biotechnology. J Biotechnol Biomater 6 (1).
Paris, D.F., Steen.W.C., Baughman, G.L., Barnett, J.T., 1981. Second-order model to predict microbial degradation of organic compounds in natural waters. Appl. Environ. Microbiol. 41 (3), 603–609.
Pennington, L.D., Moustakas, D.T., 2017. The necessary nitrogen atom: a versatile high-impact design element for multiparameter optimization. J. Med. Chem. 60 (9), 3552–3579.
Perales, J.A., Manzano, M.A., Sales, D., Quiroga, J.A., 1999. Biodegradation kinetics of LAS in river water. Int. Biodeterior. Biodegradation 43 (4), 155–160.
Pirovano, A., Huijbregts, M.A.J., Ragas, A.M.J., Veltman, K., Hendriks, A.J., 2014. Mechanistically-based QSARs to describe metabolic constants in mammals. Atla-Alternat. Lab. Anim. 42 (1), 59–69.
Popovic, M., 2019. Thermodynamic properties of microorganisms: determination and analysis of enthalpy, entropy, and Gibbs free energy of biomass, cells and colonies of 32 microorganism species. Heliyon 5 (6).
Posthuma, L., van Gils, J., Zijp, M.C., van de Meent, D., de Zwart, D., 2019b. Species sensitivity distributions for use in environmental protection,assessment, and management of aquatic ecosystems for 12 386 chemicals. Environ. Toxicol. Chem. 38, 905–917.
Poursat, B.A.J., van Spanning, R.J.M., de Voogt, P., Parsons, J.R., 2019. Implications of microbial adaptation for the assessment of environmental persistence of chemicals. Crit. Rev. Environ. Sci. Technol.
Quiroga, J.M., Sales, L.I.R.D., Nebot, E., 1994. Kinetic model development for aerobic treatment of wine vinasse. Chem. Biochem. Eng. Q. 2, 53–61.
Quiroga, J.M., Perales, J.A., Romero, L.I., Sales, D., 1999. Biodegradation kinetics of surfactants in seawater. Chemosphere 39 (11), 1957–1969.
Renata, H.W., Wang, Z.J., Arnold, F.H., 2015. Expanding the enzyme universe: accessing non-natural reactions by mechanism-guided directed evolution. Angew. Chem. Int. Ed. 54 (11), 3351–3367.
Rios-Miguel, A.B., Jetten, M.S.M., Welte, C.U., 2021. Effect of concentration and hydraulic reaction time on the removal of pharmaceutical compounds in a membrane bioreactor inoculated with activated sludge. bioRxiv.
Rodríguez, A., et al., 2020. Omics Approaches to Pesticide Biodegradation. Curr. Microbiol. 77 (4), 545–563.
Romero, L.I., 1991. Desarrollo De Un Modelo Matemático General Para Los Procesos fermentativos: Cinética De La Degradación Anaerobia. University of Cadiz, Spain, Serv. Pub. Univ. Cadiz.
Rorije, E., Langenberg, J.H., Richter, J., Peijnenburg, W.J., 1995. Modeling reductive dehalogenation with quantum chemically derived descriptors. SAR QSAR Environ. Res. 4 (4), 237–252.
Rucker, C., Kummerer, K., 2012. Modeling and predicting aquatic aerobic biodegradation - a review from a user's perspective. Green Chem. 14 (4), 875–887.
Rudik, A.V., Dmitriev, A.V., Lagunin, A.A., Filimonov, D.A., Poroikov, V.V., 2016. Prediction of reacting atoms for the major biotransformation reactions of organic xenobiotics. J. Cheminform. 8, 68.
Sathishkumar, P., et al., 2020. Occurrence, interactive effects and ecological risk of diclofenac in environmental compartments and biota - a review. Sci. Total Environ. 698, 134057.
Sathishkumar, P., et al., 2021. Persistence, toxicological effect and ecological issues of endosulfan – a review. J. Hazard. Mater. 416, 125779.
Saylor, B.T., et al., 2012. A structural element that facilitates proton-coupled electrontransfer in oxalate decarboxylase. Biochemistry 51, 2911–2920.
Schwahn, K., Beleggia, R., Omranian, N., Nikoloski, Z., 2017. Stoichiometric correlation analysis: principles of metabolic functionality from metabolomics data. Front. Plant Sci. 8, 2152.

Sharma, G., et al., 2021. Adsorptional-photocatalytic removal of fast sulphon black dye by using chitin-cl-poly(itaconic acid-co-acrylamide)/zirconium tungstate nanocomposite hydrogel. J. Hazard. Mater. 416, 125714.
Sharma, S.K., A, C., RV, S., 2008. Gray chemistry verses green chemistry: challenges and opportunities. Rasayan J. Chem. 1 (1), 68–92.
Shitut, S., Ahsendorf, T., Pande, S., Egbert, M., Kost, C., 2017. Metabolic coupling in bacteria. Environ. Microbiol. 21 (4), 1306–1320.
Smeaton, C.M., Van Cappellen, P., 2018. Gibbs Energy Dynamic Yield Method (GEDYM): predicting microbial growth yields under energy-limiting conditions. Geochim. Cosmochim. Acta 241, 1–16.
Sousa, F.L.,ThiergartT., Landan, G., Nelson-Sathi, S., Pereira, I.A.C., Allen, J.F., Lane, N., Martin, W.F., 2013. Early bioenergetic evolution. Philos. Trans. R. Soc. Lond. B 368, 1622.
Sousa, T., Mota, R., Domingos, T., Kooijman, S.A., 2006. Thermodynamics of organisms in the context of dynamic energy budget theory. Phys. Rev. E 74 (5 Pt 1), 051901.
Sreedhara, A., Freed, J.D., Cowan, J.A., 2000. Efficient inorganic deoxyribonucleases. Greater than 50-million-fold rate enhancement in enzyme-like DNA cleavage. J. Am. Chem. Soc. 122 (37), 8814–8824.
Stoddart, A.K., Schmidt, J.J., Gagnon, G.A., 2016. Biomass Evolution in Full-Scale Anthracite-Sand Drinking Water Filters Following Conversion to Biofiltration. J Am Water Works Assoc 108 (12), E615–E623.
Strous, M., Heijnen, J.J., Kuenen, J.G., Jetten, M.S.M., 1998. The sequencing batch reactor as a powerful tool for the study of slowly growing anaerobic ammonium-oxidizing microorganisms. Appl. Microbiol. Biotechnol. 50 (5), 589–596.
Struijs, J., 2020. Application of SimpleTreat 4.0 in European Substance Regulations. National Institute of Public Health and the Environment Bilthoven, The Netherlands.
Swinnen, I.A., Bernaerts, K., Dens, E.J., Geeraerd, A.H., Van Impe, J.F., 2004. Predictive modelling of the microbial lag phase: a review. Int. J. Food Microbiol. 94 (2), 137–159.
Teusink, B., Molenaar, A.W.D., Francke, C., de Vos, W.M., Siezen, R.J., Smid, E.J., 2006. Analysis of growth of Lactobacillus plantarum WCFS1 on a complex medium using a genome-scale metabolic model. J. Biol. Chem. 281 (52), 40041–40048.
Thouand, G., Durand, M.J., Maul, A., Gancet, C., Blok, H., 2011. New concepts in the evaluation of biodegradation/persistence of chemical substances using a microbial inoculum. Front Microbiol 2, 164.
Trapp, S., Brock, A.L., Nowak, K., Kastner, M., 2018. Prediction of the formation of biogenic nonextractable residues during degradation of environmental chemicals from biomass yields. Environ. Sci. Technol. 52 (2), 663–672.
UnitedNations, 2011. Globally Harmonized System of Classification and Labelling of Chemicals (GHS). ST/SG/AC.10/30/Rev.4, New York and Geneva.
USEPA United States Environmental Protection Agency, Washington, DC, USA, 2012. EPI Suite Estimation Programs Interface Suite™ for Microsoft® Windows, v 4.11.
van Bergen, T.J.H.M., et al., 2020. Do initial concentration and activated sludge seasonality affect pharmaceutical biodegradation rate constants? Applied Microbiology and Biotechnology 105, 6515–6527.
van Lier, J.B., Mahmoud, N., Zeeman, G., 2008. Chapter 16: Anaerobic Wastewater Treatment, Biological Wastewater Treatment: Principles Modelling and Design. IWA Publishing, London UK.
Van Briesen, J.M., 2001. Thermodynamic yield predictions for biodegradation through oxygenase activation reactions. Biodegradation 12 (4), 265–281.
Van Briesen, J.M., 2002. Evaluation of methods to predict bacterial yield using thermodynamics. Biodegradation 13 (3), 171–190.
Vlastaridis, P., et al., 2017. The pivotal role of protein phosphorylation in the control of yeast central metabolism. G3 (Bethesda) 7 (4), 1239–1249.
von Stockar, U., Liu, .J..-S., 1999. Does microbial life always feed on negative entropy? Thermodynamic analysis of microbial growth. Biochim. Biophys. Acta (BBA) 1412 (3), 191–211.
Vrede, K., Heldal, M., Norland, S., Bratbak, G., 2002. Elemental composition (C, N, P) and cell volume of exponentially growing and nutrient-limited bacterioplankton. Appl. Environ. Microbiol. 68 (6), 2965–2971.
Vrijheid, M., Casas, M., Gascon, M., Valvi, D., Nieuwenhuijsen, M., 2016. Environmental pollutants and child health-A review of recent concerns. Int. J. Hyg. Environ. Health 219 (4–5), 331–342.
Walkiewicz, K., Cardenas A.S.B., Sun, C., Bacorn, C., Saxer, G., Shamoo, Y., 2012. Small changes in enzyme function can lead to surprisingly large fitness effects during adaptive evolution of antibiotic resistance. Proc. Natl. Acad. Sci. U.S.A. 109 (52), 21408–21413.
Wang, J., et al., 2021. Towards a systematic method for assessing the impact of chemical pollution on ecosystem services of water systems. J. Environ. Manag. (revision).
Westerhoff, H., van Dam, K., 1987. Thermodynamics and Control of Biological Free-Energy Transduction. Elsevier.
Westerhoff, H.V., Lolkema, J.S., Otto, R., Hellingwerf, K.J., 1982. Thermodynamics of growth - non-equilibrium thermodynamics of bacterial-growth - the phenomenological and the mosaic approach. Biochim. Biophys. Acta 683 (3–4), 181–220.
Yagi, N., Kenmotsu, H., Sekikawa, H., Takada, M., 1991. Studies on the photolysis and hydrolysis of furosemide in aqueous solution. Chem. Pharm. Bull. 39 (2), 454–457.
Yang, Y.L., et al., 2020. Occurrence of free amino acids in the source waters of Zhejiang Province, China, and their removal and transformation in drinking water systems. Water, 12 (1).
Young, L.Y.P., C, D., 2005. Metabolic Biomarkers for monitoring in situ anaerobic hydrocarbon degradation. Environ. Health Perspect. 113 (1), 62–67.
Yuan, Z., VanBriesen, J.M., 2002. Yield prediction and stoichiometry of multi-step biodegradation reactions involving oxygenation. Biotechnol. Bioeng. 80 (1), 100–113.
Zhang, D., et al., 2016. Characterization of microbial communities in wetland mesocosms receiving caffeine-enriched wastewater. Environ. Sci. Pollut. Res. Int. 23 (14), 14526–14539.